European Coordination for Accelerator Research and Development

PUBLICATION

Report on HOM experimental methods and code

Shinton, I R R (UMAN) *et al*

19 June 2014

The research leading to these results has received funding from the European Commission under the FP7 Research Infrastructures project EuCARD, grant agreement no. 227579.

This work is part of EuCARD Work Package **10: SC RF technology for higher intensity proton accelerators and higher energy electron linacs**.

The electronic version of this EuCARD Publication is available via the EuCARD web site <http://cern.ch/eucard> or on the CERN Document Server at the following URL : <http://cds.cern.ch/record/1710321

Grant Agreement No: 227579

EuCARD

European Coordination for Accelerator Research and Development

Seventh Framework Programme, Capacities Specific Programme, Research Infrastructures, Combination of Collaborative Project and Coordination and Support Action

DELIVERABLE REPORT

REPORT ON HOM EXPERIMENTAL METHODS AND CODE

DELIVERABLE: D10.5.2

Document identifier:	EuCARD-Del-D10.5.2-final
Due date of deliverable:	End of Month 52 (July 2013)
Report release date:	29/07/2013
Work package:	WP10: Superconducting Radio Frequency Technology
Lead beneficiary:	UMAN
Document status:	FINAL

Abstract:

Experimental methods and various codes used are reported on with the aim to understand the signals picked up from the higher order modes in the third harmonic cavities within the ACC39 module at FLASH. Both commercial computer codes have been used, and also codes written for the express purpose of understanding the sensitivity of the modal profiles to geometrical errors and other sources of experimental errors.

The European Coordination for Accelerator Research and Development (EuCARD) is a project co-funded by the European Commission in its 7th Framework Programme under the Grant Agreement no 227579. EuCARD began in April 2009 and will run for 4 years.

Delivery Slip

	Name	Partner	Date
Authored by	I.R.R. Shinton, P. Zhang and T. Flisgen	UMAN, DESY, UROS	9/6/2013
Reviewed by	R. M. Jones, N. Baboi and U. van Rienen	UMAN, DESY, UROS	11/06/2013
Approved by WP Coordinator	O. Napoly	CEA	13/06/2013
Approved by Project coordinator	Jean-Pierre Koutchouk		26/07/2013

TABLE OF CONTENTS

1. EXECUTIVE SUMMARY

The higher order modes (HOM) in the third harmonic cavities at FLASH can dilute the emittance of the accelerated beams if they are not properly suppressed. The motivation of this work is to monitor dipole HOMs radiated to the special damping couplers, and provide a means to align the beam and reduce the excited modes. Moreover, the signals can be used to provide diagnostic information on the beam position with the cavities.

As the modes propagate through all four cavities in the module ACC39, the HOM dampers share the mode suppression. On the other hand, the characteristic frequencies and modal distributions are very sensitive to geometrical errors (which will inevitably occur in fabricating the cavities).

We utilise computationally intensive packages which rely on parallel computing to model the complete 4-cavity structure. This allows the modes to be identified and some general properties of their overall distribution to be noted. However, as small geometrical errors can modify the distribution we have relied on a global scattering matrix (GSM) method as well as on Coupled S-parameter Calculations (CSC) to rapidly determine the sensitivity to errors. We developed our own codes for this expressed purpose. The S-parameter calculations are compared in a rigorous manner with measurements conducted at FLASH. Additionally, the frequency domain concatenation algorithm CSC has been transferred to time domain. Moreover, the influence of the beam is accounted in this new scheme, denoted as Coupled Transient Calculations (CTC). Thus, using CTC, transient beam excited port signals in large structures can be computed very efficiently on standard workstations.

The simulations helped to understand the modal spectrum of the module ACC39. In particular, they provided useful modal candidates for the HOM beam position monitor system. Moreover, a comparison between measured and simulated S-parameters for a four cavity system with symmetry breaking HOM couplers over a wide frequency range has been made for the first time in the framework of WP 10.5.

An overview of the GSM, CSC and the CTC scheme is provided, together with some results on the ACC39 module, with and without experimental errors. These simulations are compared to large scale finite element simulations, and also to experimental measurements. The comparisons show that the results obtained by the different concatenation schemes agree remarkable. Moreover, the simulations fit to the conducted measurements in a reasonable manner.

In addition, sub-tasks 10.5.2 and 10.5.3 were involved in measurements with beam at the FLASH facility. In comparison to WP 10.5.1 a different hardware setup is employed to analyse the HOM port signals. The main advantage of this alternative approach is that it needs fewer electronic components.

2. INTRODUCTION

The ACC39 third harmonic cavities have been designed and fabricated by FNAL and DESY. They are used in the FLASH linac and to be used at the European XFEL facility at DESY to minimise the energy spread along the bunches. The higher order modes (HOMs) in this module have the potential to cause significant emittance dilution if they are not sufficiently suppressed. Probe and beam based experiments have indicated significant discrepancies

between modes predicted in stand-alone 9-cell cavities compared to those in 4-cavity modules. We seek to understand the nature of the HOMs within this structure with the primary purpose both understanding the HOMs in ACC39, to prevent emittance dilution and the possibility of developing a HOM BPM system for ACC39 similar to the existing HOM BPM system already used to align the beam at FLASH in the main TESLA accelerating linac modules.

3. BACKGROUND REVIEW

FLASH is a self-amplified spontaneous emission free electron laser delivering ultra-short laser-like pulses with a wavelength between about 4.5 and 47 nm. It is a user and a test facility. Fig. 1 shows the main components of the linac. A photoelectric gun generates trains of electron bunches, which are accelerated to up to 1200 MeV by 8 accelerating modules, each containing eight super-conducting 1.3 GHz TESLA cavity strings. Two bunch compressors reduce the length of each bunch to the order of hundreds of femtoseconds. Four 3rd harmonic cavities working at 3.9 GHz are used to linearize the longitudinal phase space, just after the booster section. The beam passes through transverse and energy collimators and then through undulators to produce laser pulses. The photons continue to the FEL experimental hall, while the electron beam is finally sent to the energy dump. The bunch charge used is between 100 pC and 1 nC. The pulses are up to 800 µs long and have a repetition frequency of 10 Hz and the bunch repetition frequency (within the pulses) is up to 1 MHz. A schematic layout of FLASH is presented in Fig. 1.

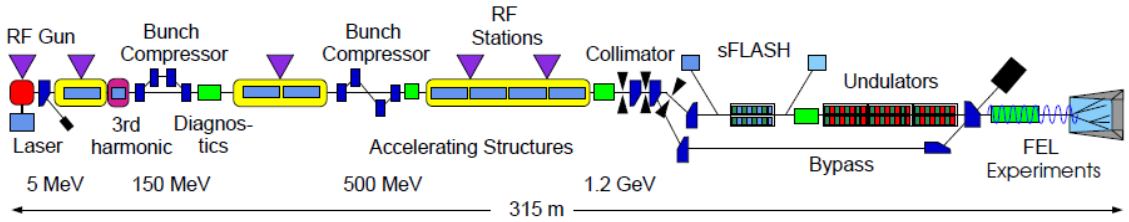

Fig. 1 Diagrammatic layout of FLASH, the location of the third harmonic cavity is circled in red (Diagram courtesy DESY).

In operating a FEL an energy variation along the length of an accelerated bunch adversely affects the generation of radiation. The cosine fields used to accelerate these bunches at FLASH or XFEL introduce an energy spread over the length of the bunch. It is desirable to reduce this energy spread by flattening the overall field and this can be achieved by including harmonics of the fundamental frequency of the linac. A single frequency operating at the nth harmonic can be used to flatten out the dependence of the energy gain versus phase by cancelling the second derivative of the fundamental at its peak.

In practice the first component in a Fourier expansion is used, namely the 3rd harmonic. This minimises the effect of transverse wakefields which grow proportionately to the third power in frequency (this is discussed further in the next section). The third harmonic module operates in the decelerating phase in conjunction with the ACC1 module, this provides linearization of the radio frequencies (RF) acceleration field with time over the duration of the beam bunching. Consider a triangular wave, with this waveform off crest acceleration would result in the desired linear dependence (the beam would be linearly chirped). This triangular wave can be described as an infinite series of cosine waves as seen in Eq. 1 in which Φ is the phase and n is the odd harmonic frequencies

$$f(\phi) = \frac{8}{\pi^2} \sum_n \frac{1}{n^2} \cos(n\phi). \quad (1)$$

Hence by choosing the appropriate phasing to the fundamental RF system and adding the third harmonic RF, regions with a linear voltage chirp can be obtained. An idealised RF linearization around the phase of the operational beam Φ_{beam} is produced by adjusting the phase of the third harmonic cavity Φ_{3rd} as:

$$\phi_{3rd} = \pi + 3\phi_{beam}. \quad (2)$$

As well as adjusting the third harmonic amplitude V_{3rd} with respect to the main accelerating amplitude V_{rf} as:

$$V_{3rd} = \frac{1}{9} V_{rf}. \quad (3)$$

The resulting voltage summation v_{rf} can then be written as:

$$v_{rf}(\phi) = V_{rf} \left(\cos\phi + \frac{V_{3rd}}{V_{rf}} \cos(3\phi - \phi_{3rd}) \right). \quad (4)$$

The effect of the linearization of the third harmonic cavity is illustrated in Fig. 2a) and b) in which Φ_{beam} = -12°.

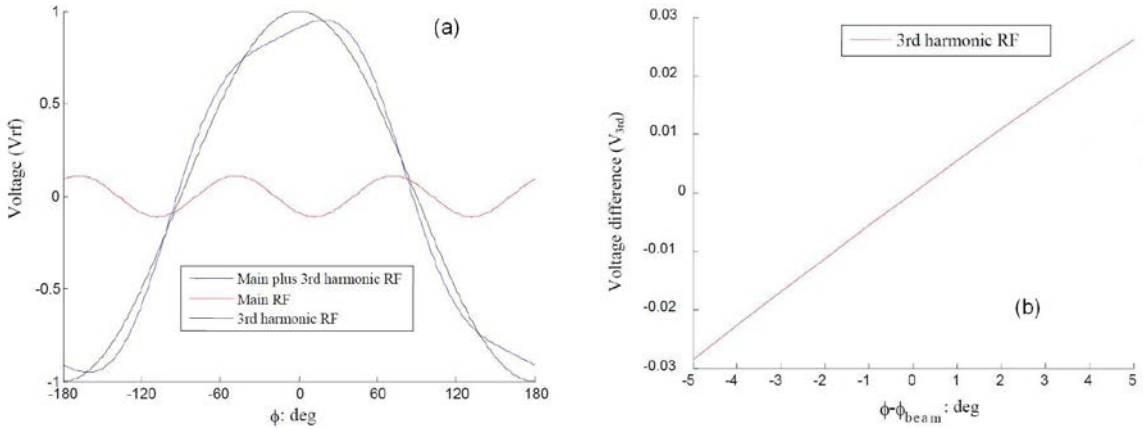

Fig. 2 a) Comparison of the RF voltages normalised to the fundamental RF amplitude, here a decelerating voltage chirp of 12° has been applied. b) The resulting linearization obtained with the third harmonic cavities shown as "Main plus 3rd harmonic RF" in (a) is a direct result of the second half of equation 4, which is the 3rd harmonic RF producing the voltage chirp as shown.

Finally we note that flattening the field also reduces the growth of transverse phase space. The transverse magnetic fields arise from the rate of change of the longitudinal electric field. Thus, flattening the electric field will also result in a reduced magnetic field. Hence the use of a cryo-module of third harmonic cavities will reduce the dilution of both longitudinal and transverse phase space. This method is currently being used at FLASH and will also be used at XFEL, DESY to compensate for an energy spread across the bunch. The bunch shaping module consists of four nine-cell cavities operating at 3.9 GHz has been designed and built by FNAL (illustrated in Fig. 3 and Fig. 4).

Fig. 3 Schematic of FNAL cryo-module consisting of four 3.9 GHz cavities (Diagram courtesy FNAL).

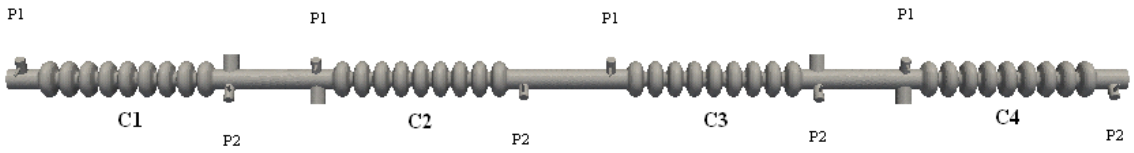

Fig. 4 Schematic representation of the 4 cavities within ACC39. The power couplers are placed downstream for cavities 1 and 3 (C1 and C3) and upstream for C2 and C4.

The naming convention of the cavities and ports of ACC39 used in this report is depicted in Fig. 4. We will define the naming convention as follows c1p1, c4p2 refers to the transmission from HOM p1 of cavity C1 to the HOM p2 of cavity C4.

Due to the lack of space available for the installation of ACC39 into the FLASH architecture (a shorter module was required) the cavities were installed in the diagrammatic representation in Fig 5 (C1 and C2 power couplers horizontally facing each other). Note that in this configuration a residual kick remains for the beam on axis.

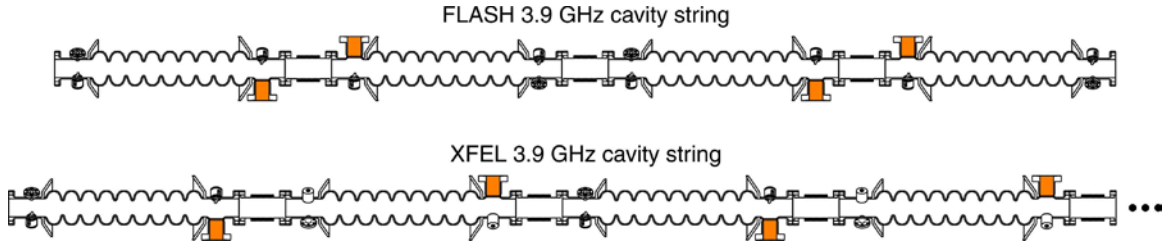

Fig. 5 Diagrammatic representation of an ACC39 module configuration within FLASH and XFEL, here the power couplers have been highlighted in orange (Diagram courtesy E. Vogel).

4. MOTIVATION OF HOM STUDY

An electron beam moving through a superconducting accelerating cavity will produce an electromagnetic 'wake'. Short range fields produced by the head of the bunch can interact on the tail resulting in a degradation of the quality of the beam in which the longer range fields can act on subsequent bunches. In the worst case, these fields may be resonant with the inter-bunch spacing, causing beam blow up (BBU). These wake fields can be represented as a multi-pole series (in the cylindrically symmetric geometry of the cavities), each term in this series may be classified according to its azimuthal symmetry as being either monopole,

dipole, quadrupole, or higher order in nature, often referred to as higher order modes (HOM). Most of these HOMs (dipole modes for example) will exist in two orthogonal polarisations, and that the degree of frequency splitting of these modes is related to 'asymmetries' in the cavity design which include manufacturing errors, miss-alignments and the presence of RF couplers. The HOMs therefore can potentially damage the beam quality, and their effects must be reduced through careful design of the bandwidth of the cavity (i.e. the tolerance to machining errors) and the inclusion of HOM couplers to extract and damp these modes. The HOM couplers are genuinely designed as wideband devices to extract the power of the HOMs, but with a tunable bandstop filter to minimise the coupling to the accelerating mode. By monitoring the output from these ports, it is, therefore, possible to monitor any modes excited by the beam that couple well to them and as a bi-product of this information can be gained as to the position of the beam and the HOMs can be used as a beam positioning monitor system (BPM). Such a system has been implemented at FLASH and is used to align the beam within the linac sections.

It is important to damp the modal components of the wakefields and to ensure there are no trapped modes with particularly high *R/Q* values. The longitudinal and transverse wakefields ($W_{//}$ and $W_{\perp}$ respectively) scale with the second and third power of the frequency respectively as

$$W_{//} \sim f^2 \qquad W_{\perp} \sim f^3 \tag{5}$$

The bunch shaping third harmonic cavities operate at 3.9 GHz, consequently they are one third the size of the accelerating 1.3 GHz TESLA cavities as seen in Fig. 6 (since the geometry scales with respect to the operating frequency). The wakefields in these third harmonic cavities are therefore considerably larger than those in the main accelerating linacs. Hence the transverse wakefields for the 3.9 GHz cavities in ACC39 will be nine times the magnitude of those of the accelerating 1.3 GHz TESLA cavities.

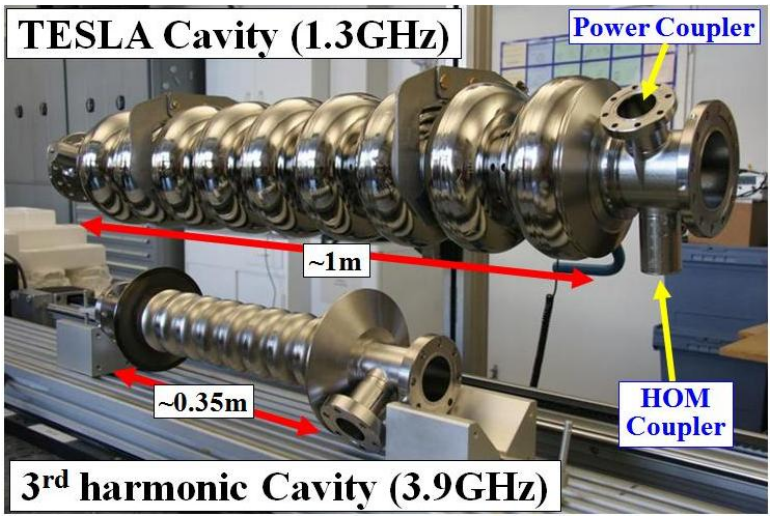

Fig. 6 TESLA cavity (upper) and third-harmonic cavity (lower). On the right side of each cavity one can see the port for the input couplers. The HOM couplers can also be partially seen at either side of the cavities (Picture courtesy DESY).

As a consequence the HOMs in ACC39 must be carefully controlled to prevent transverse emittance blow up and maintain the beam trajectory. These very HOMs could also be used as

a BPM system similar to the one already used for the FLASH main linacs. These HOMs must be adequately modelled and understood if such as system is to be designed. In the following sections we will discuss how to model ACC39 using a variety of techniques. In Section 4.1 the semi analytical globalised scattering matrix (GSM) methodology and the Coupled S-Parameter Calculation scheme (CSC) are introduced. Section 4.2 discusses the generalization of the CSC scheme to the Coupled Transient Calculation scheme (CTC). Section 4.3 presents the full numerical simulations with various finite element (FEM) software packages such as HFSS, CST and ACE3P.

4.1. THE GLOBAL SCATTERING MATRIX METHODOLOGY AND THE METHOD OF COUPLED S-PARAMETER CALCULATIONS

The global scattering matrix technique is a relatively mature RF concept, in which the scattering matrix of a junction is obtained by "cascading" two sections at a time, these individual cascaded sections will henceforth be referred to as "unit cells". There are a number of methods that can be found throughout the literature, the form used here is a 2 port GSM technique:

$$\begin{aligned} S_{11} &= S_{11}^{A}\left(U - S_{11}^{B}S_{22}^{A}\right)^{-1}S_{11}^{B}S_{21}^{A} \\ S_{12} &= S_{12}^{A}\left(U - S_{11}^{B}S_{22}^{A}\right)^{-1}S_{12}^{B} \\ S_{21} &= S_{21}^{B}\left(U - S_{22}^{A}S_{11}^{B}\right)^{-1}S_{21}^{A} \\ S_{22} &= S_{22}^{B} + S_{21}^{B}\left(U - S_{22}^{A}S_{11}^{B}\right)^{-1}S_{22}^{A}S_{12}^{B} \end{aligned} \tag{6}$$

In Eq. 6, U is the identity matrix and the superscripts of A and B represent the matrices of the individual sections to be cascaded. The technique is very efficient and can readily incorporate misalignments and cavity perturbations into the calculation. It should be noted that this technique is more robust than using an ABCD method, where the inversion of the matrices can result in numerical errors if the denominator is very small. The GSM method was chosen for its simplicity and robustness; however it is not an "N" port calculation and so to compensate for this (unless otherwise stated) any port not directly used in the cascaded calculations presented here is considered as being open (i.e. a magnetic boundary is imposed upon it). There are variations of GSM which offer "N" port calculations, however this results in an ever increasing scattering matrix size (due to the inclusion of more ports at each stage of the cascading process).

Aiming for highly reliable results, GSM is used at UMAN while another "N" port scattering matrix method, the Coupled S-Parameter Calculation scheme (CSC) being developed at UROS is used as an ideal alternative candidate for large scale S-matrix calculations. CSC is a method whereby individual S-matrices of various subsections of a large structure are combined and used to determine the amplitudes at various ports of the subsections. This method has the ability to determine the scattering properties of irregular structures (including cavities with couplers). This technique has also been applied to modelling the structure of ACC39 by UROS.

There are two types of couplers in ACC39 (illustrated in Fig. 7). In applying the GSM method, 6 main structures must be simulated (including the two couplers). In addition two input cells are needed to drive power through the structure, making a total of 8 structure types. These cells are illustrated in Fig. 7.

All the multi-moded 2-port (single cell, beam pipe), 3-port (end-cell with HOM-coupler) or 4-port (end-cell with HOM- and power coupler) scattering matrices used in the GSM method were generated using the driven modal solver of HFSS v11.2.1. Since the excitation field polarisation of a mode on a wave port in HFSS is calculated in an arbitrary direction, it is necessary to align specific modes. This is of particular importance during the cascade calculation in which the propagation of specific modes must be maintained throughout the calculation. This is achieved within HFSS by aligning specific modes with a calibration direction, which are universally applied (with respect to the chosen coordinate system) to all unit cells. An example of these calibration lines is demonstrated in Fig. 8.

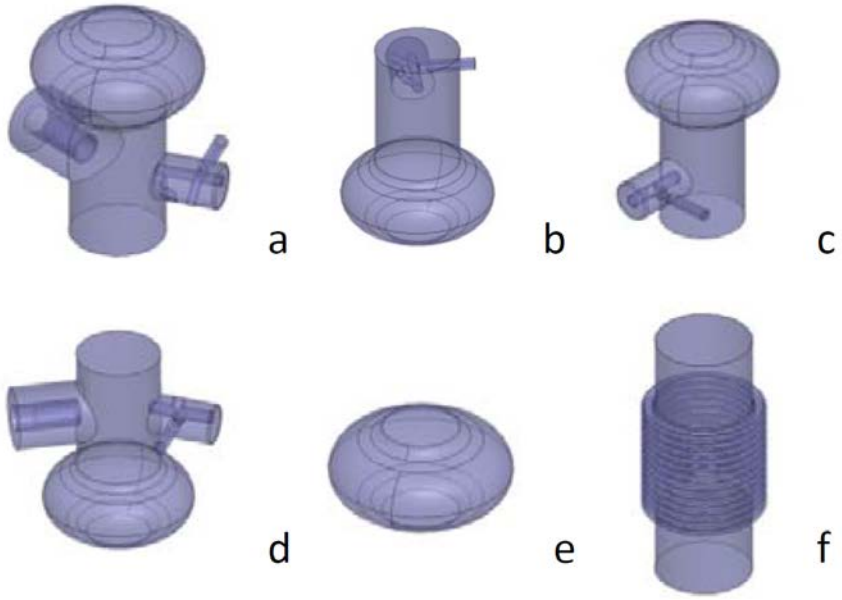

Fig. 7 Unit cells used in the cascade calculations of the FNAL ACC39 cryo-module.

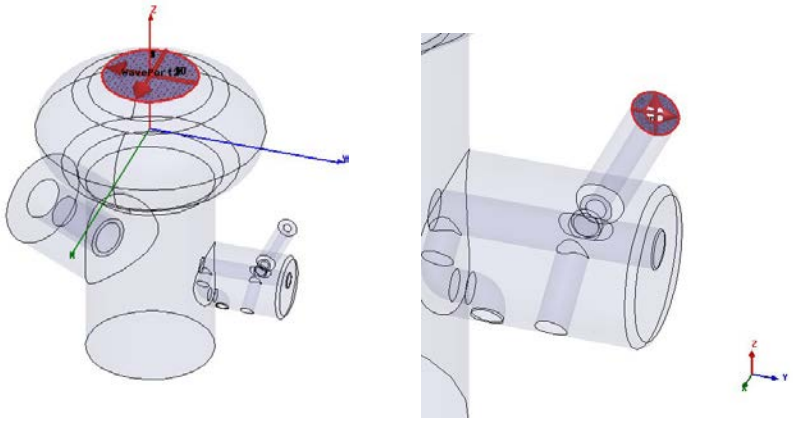

Fig. 8 Polarisation directions used in the unit cells within HFSSv11.2.1.

Furthermore in the normalisation process it is important to note that HFSS has the facility to re-normalise the port impedance to a specific impedance value (denoted by the user). This has the effect of removing the frequency dependency from the port impedances. This is implemented within HFSS using

$$Z = \sqrt{Zo}\left(I - S\right)^{-1}\left(I + S\right)\sqrt{Zo} \tag{7}$$

in which S is the $n \times n$ generalized scattering matrix, I is an $n \times n$ identity matrix and Z_o is a diagonal matrix having the characteristic impedance (Z_o) of each port as a diagonal value. The scattering matrix is readily obtained from Eq. 7 re-normalised to the port impedance.

$$S_\Omega = \sqrt{Y_\Omega}\left(Z - Z_\Omega\right)\left(Z + Z_\Omega\right)^{-1}\sqrt{Z_\Omega} \tag{8}$$

In Eq. 8 Z is the structure's unique impedance matrix and Z_Ω and Y_Ω are diagonal matrices with the desired impedance and admittance as diagonal values.

All unit cell simulations used in the GSM calculations were conducted using HFSS v11.2.1, in which a seed mesh, consisting of a surface mesh of 30 μm, with an aspect ratio of 3, and a volume mesh of 10,000 elements was used. The mesh was adaptively refined until a convergence criteria of less than 0.01% was achieved, at which point a fast frequency sweep (using an ALPS algorithm) was made at the upper limit of the frequency range of interest with 1 MHz frequency steps, and with 20 modes per port. A fast frequency sweep was chosen over the more robust (albeit slower) discrete frequency sweep as it accelerates the generation of results by a factor of 10 or more. Due to the inherent stability requirements of the ALPS algorithm, all simulations were cross-checked against a discrete frequency sweep (in which a larger frequency step was used). In addition to GSM we also use the ACE3P computational suite to simulate ACC39 in its entirety, the capabilities of this powerful numerical code are introduced to the reader in the next section. To demonstrate the validity of the GSM method we present a benchmarking problem in which the GSM calculation is compared to a full structure simulation in HFSS. This is shown below in Fig 9 in which we propagate modes from the HOM port of C1 through to the iris of a middle cell. We observe excellent agreement between the GSM method and the full scale simulation. This gives some confidence in the GSM method and allows progression on to simulating the 3.9 GHz module in its entirety; the results of which are presented in the next section.

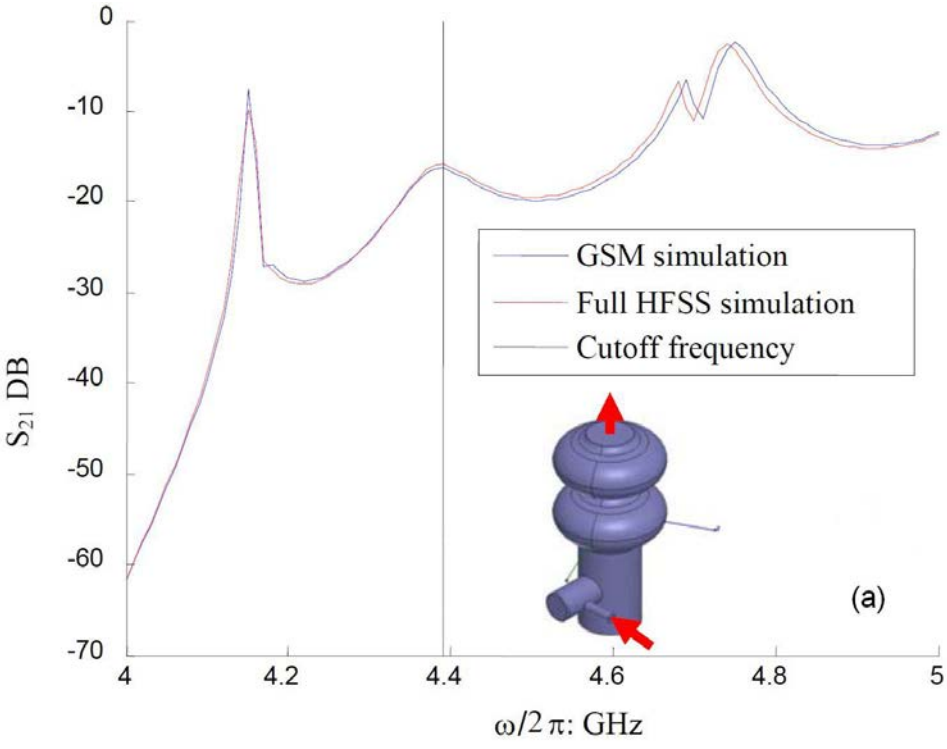

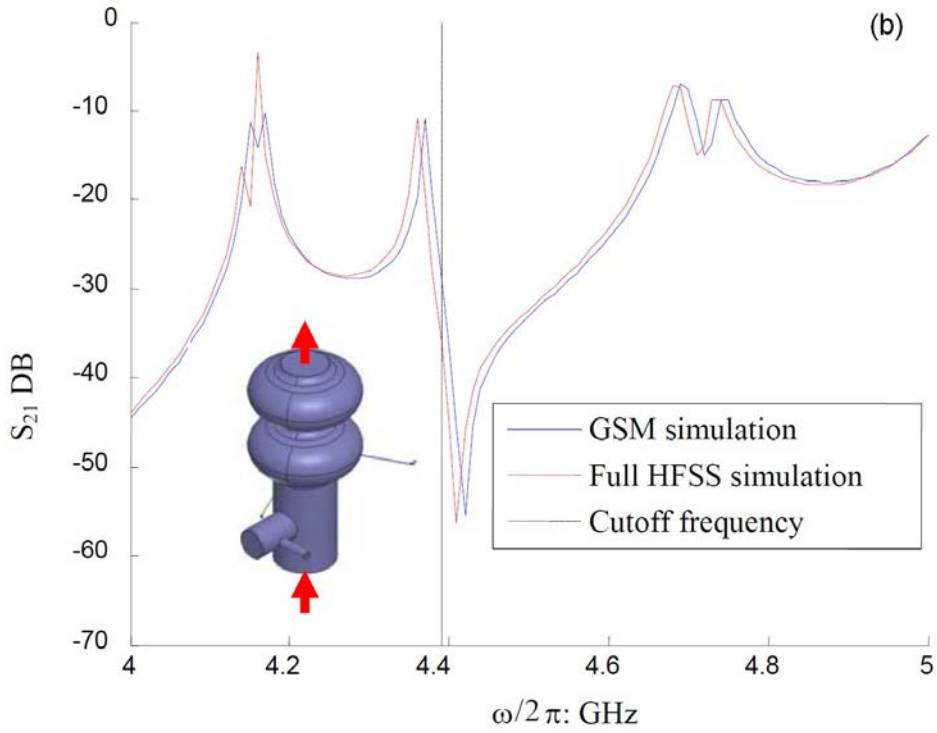

Fig. 9 Benchmarking comparison for the dominant mode propagating into the TE_{11} mode between a full HFSS v11.2.1 simulation and that calculated by GSM. The structure being simulated is shown insert with red arrows indicating the ports used to drive the simulations. The dashed black line represents the beam-pipe cut-off.

It is important to bear in mind that the GSM approach requires at least a single mode to be propagating within the input and output ports. TEM modes clearly satisfy these criteria. Below 4.39 GHz the agreement between simulation and experiment is poor. We attribute the discrepancy in the results as being due to modes below cut-off (the beam-pipe cut-off is ~4.39 GHz for dipole modes) in the cascaded blocks. The method relies on there being at least one propagating mode present in order to be accurate as can be seen in Fig. 9 for the propagation of the TE_{11} to TE_{11} below cut-off, in which a very large number of evanescent modes would be required to be included in the calculation in order to improve the accuracy.

4.2. COUPLED TRANSIENT CALCULATIONS

The methodologies GSM and CSC do not account for ports inside the structure, namely the bunches of charged particles traversing it. Moreover, GSM and CSC are restricted to frequency domain and cannot model the transient processes of HOM excitation. Therefore, CSC scheme has been generalised to incorporate the influence of sufficiently stiff beams (field equations and equations of motion are decoupled). Consequently, the scattered wave amplitudes of the kth segment are described by the commonly known scattering matrix plus a term accounting for the beam excited fields in the structure:

$$b_k(j\omega) = S_k(j\omega)a_k(j\omega) + y_k(j\omega). \tag{9}$$

The modified ansatz (9) is put into the CSC formalism to obtain

$$b_{sct}(j\omega) = S_{\mathrm{csc}}(j\omega)a_{sct}(j\omega) + M_{beam}(j\omega)y_{\mathrm{int}}(j\omega) + y_{sct}(j\omega). \tag{10}$$

The quantity on the left hand side collects the amplitudes of the waves, which are scattered into the waveguide ports of the full structure (e.g. the HOM port signals). The first

contribution on the right hand side of (10) describes the relationship between incident and scattered waveguide signals of the concatenated structure (common S-matrix description of full structure). The last two contributions on the right hand side of (10) reflect the influence of the beam driven signals of the substructures on the scattered waveguide port signals of the concatenated structure. As a matter of fact, it is not possible to compute the matrices $S_{\mathrm{csc}}(j\omega)$ and $M_{beam}(j\omega)$ in general, because this implies the knowledge of the scattering properties of the individual segments on an infinite frequency interval. Nonetheless, these matrices can be computed in a finite frequency range, sampled on discrete frequencies, if the S-parameters of the segments are known in a frequency range, sampled on discrete frequency nodes. This frequency range may be adjusted by experimental needs. As mentioned before, CSC does not consider beam excited signals. Since CTC is a generalization of CSC, the latter is included in Eq. (10) if the beam excited signals $y_{\mathrm{int}}(j\omega)$ and $y_{sct}(j\omega)$ are set to zero, which means that no interaction between beam and structure takes place. Yet, the focus of the investigations lies on the computation of beam driven port signals of large structures. In consequence, signals which are incident on that large structure are typically set to zero i.e. $a_{sct}(j\omega)=0$.

As a matter of fact, equation (10) describes the dependencies in frequency domain. Transferring the equation to time domain leads to the convolution

$$b_{sct}(t) = M_{beam}(t) * y_{\mathrm{int}}(t) + y_{sct}(t). \tag{11}$$

To avoid the direct evaluation of the convolution, a linear time-invariant system with multiple inputs and outputs is created by means of pole fitting, so that this system approximates the frequency domain behaviour of (10) in a finite frequency range. The response of this system due to the stimulus $y_{\mathrm{int}}(t)$ is computed using standard ordinary differential equation solvers, whereas the final addition of this response to $y_{sct}(t)$ to compute $b_{sct}(t)$ is straightforward. It is spotlighted that the signals $y_{sct}(t)$ and $y_{\mathrm{int}}(t)$ are determined by an external wakefield solver like e.g. CST MICROWAVE STUDIO® (CST MWS).

Figure 10 shows the proof of concept for CTC using two coupled cylindrical resonators.

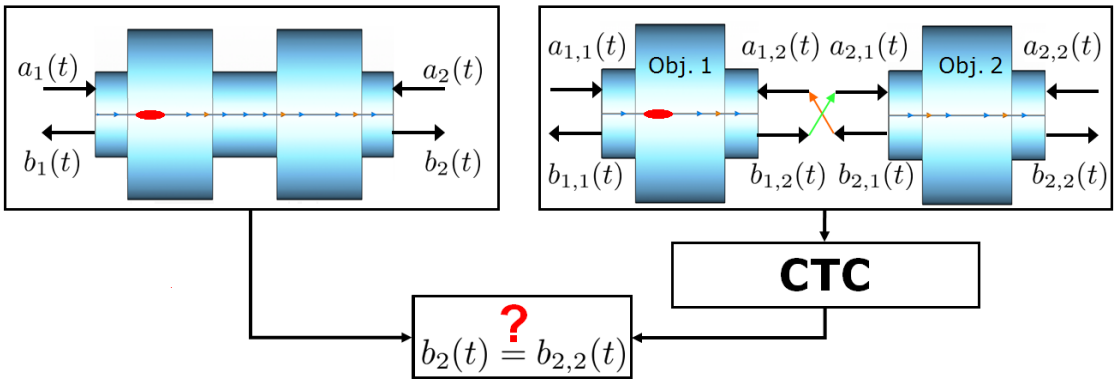

Fig. 10 Comparison between direct computation vs. element-wise computation and concatenation using CTC.

The structure is chosen such that a direct computation of the beam induced port signals is easily feasible. Figure 11 shows the comparison between direct computation and element-wise computation. It is observable that the beam driven port signal, acquired by the straightforward computation (blue plot) is almost identical to the signal obtained by element-wise computation followed by the CTC concatenation (red plot).

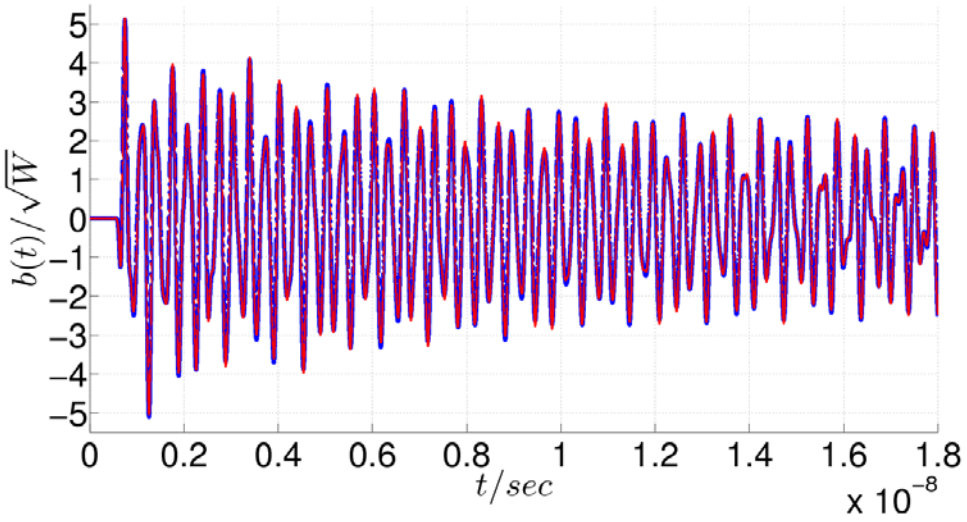

Fig. 11 Comparison between direct computation $b_2(t)$ *(blue curve) and element-wise computation of signal contributions and coupling using CTC* $b_{2,2}(t)$ *(red curve).*

It is worth to mention that CTC is currently further developed to obtain a formulation which is based on the eigenmodes of the individual sections and not on frequency domain scattering parameters and beam excited transient signals of the individual sections. This should further speed up the simulations.

4.3. THE ACE3P COMPUTATIONAL SUITE

The electromagnetic computational suite "ACE3P" has been developed by the ACD group at SLAC over the past 20 years, and is capable of large scale parallel computational simulations. ACE3P consists of the following modules: OMEGA3P an frequency domain solver, S3P a driven modal solver, T3P a time domain solver, Track3P a particle tracking code used for multi-pacting simulations, PIC3P a particle in cell solver and TEMP3P a thermal and structural effects simulator.

ACE3P has been developed for the main purpose of simulating accelerating structures and associated devices. It is a modular code in that it relies on external components for certain features. All the meshing used in ACE3P is generated using the code CUBIT and the visualization of the electromagnetic field quantities calculated from the ACE3P suite is done using the processing program PARAVIEW.

Omega3P can be used to: optimize RF parameters; reduce peak surface fields; determine HOM damping, trapped modes and their heating effects; design dielectric and ferrite dampers. S3P calculates the transmission (*S* parameters) in open structures. T3P uses a driving bunch to: evaluate the broadband impedance, trapped modes and signal sensitivity; compute the wakefields of short bunches with a moving window; simulate the beam transit in large 3D complex structures. Track3P studies: multi-pacting in cavities and couplers by identifying multi-pacting barriers and sites; dark current in high gradient structures including transient effects. Pic3P calculates the beam emittance in RF gun designs.TEM3P computes integrated EM, thermal and structural effects for normal and superconductive cavities with nonlinear temperature dependence.

In the simulations of ACC39 conducted in this paper we utilize the following features of the ACE3P suite: the frequency domain code Omega3P to determine resonant modes; the driven modal S3P solver to calculate the scattering parameters; and T3P to simulate the effect of the beam. Note that the bellows sections are neglected in these initial simulations in order to obtain rapid results.

5. SIMULATIONS AND MEASUREMENTS OF HOM SPECTRA

From our previous GSM and CSC coupled cavity simulations we observe the effects of the splitting of the modes as a result of the couplers and the strong coupling between neighbouring cavities. Interference effects are evident in which there is coupling through the beam-pipes of the dipole modes in adjacent cavities (giving rise to the additional resonances observed), thus we are able to simulate the effects of these multi-cavity modes. Hence in order to accurately simulate ACC39 it must be considered in its entirety instead of the previously investigated idealised single cavity studies, this aspect is investigated in Section 5.1.

5.1. MODULE BASED EIGEN MODE SIMULATIONS AND MEASUREMENTS

In order to develop a HOM BPM system for ACC39 it is necessary to establish the electromagnetic field distribution of these multi-cavity modes for ACC39 in its entirety for the reasons established in the last two sections. Through the use of GSM the scattering matrices of the entire structure can be simulated, matching and misalignment errors can be rapidly incorporated within these simulations. However it is difficult to properly obtain the complete field within these coupled structures and in particular to identify trapped modes. We utilized the frequency domain code Omega3P, part of the ACE3P suite, to obtain the modes of the entire structure. The bellows sections are neglected in these initial simulations in order to obtain rapid results. We analysed over 1200 modes in the range of 3 GHz to 10 GHz, in which the full structure used in the simulations is depicted in Fig. 12. The bellows were not considered in the calculation (as they are computationally expensive to simulate). The mesh generated using CUBIT for use with Omega3P was a third order mesh consisting of more than 3 million elements.

Fig. 12 Sample of ACE3P output (displayed in Paraview) showing the 3D magnitude of the electric field distributions of the trapped mode at 9.061 GHz from the 5th dipole band.

The majority of the modes in the cryo-module are able to propagate out through the beam tubes. Here we focus on the properties of the modes which are trapped in either the cavity or the beam-pipe region. Eigenmodes determined with Omega3P simulations that are largely restricted to the beam-pipe region are illustrated in Fig. 13, together with an experimental measurement of the transmission through the couplers in which the beam is moved horizontally and vertically. In the data illustrated, variation from the second cavity out of the string was monitored.

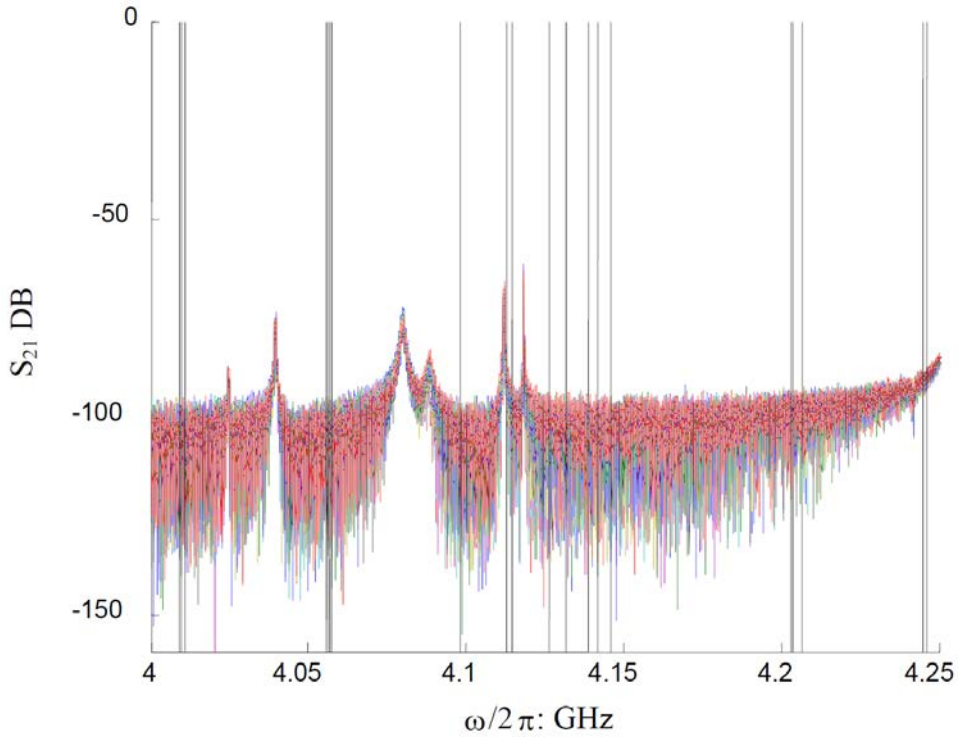

Fig. 13 Comparison of 1st beam-pipe mode band experimental RSA data (in which beam moved with cross offset – various colours relate to different offsets) to ACE3P eigenvalues (black lines).

The field profile for a selected set of modes in this band is illustrated in Fig. 14. It is evident that these are indeed beam-pipe modes. However the degree to which they couple to the beam, represented by *R/Q* is rather weak.

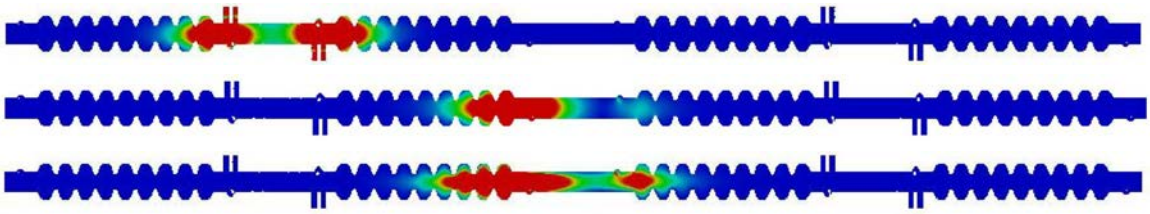

Fig. 14 ACE3P magnitude electric field distribution from the 1st beam-pipe mode band: 4.056 GHz (top), 4.126 GHz (middle) and 4.142 GHz (bottom).

The next most promising region for a HOM based BPM system is the 5th dipole band, which from the initial idealised 9-cell simulations demonstrated that there were potentially trapped modes in this region. Once again we observe that there are several modes predicted by ACE3P that coincide with the experimental data and show a linear dependence in beam offset in Fig. 15.

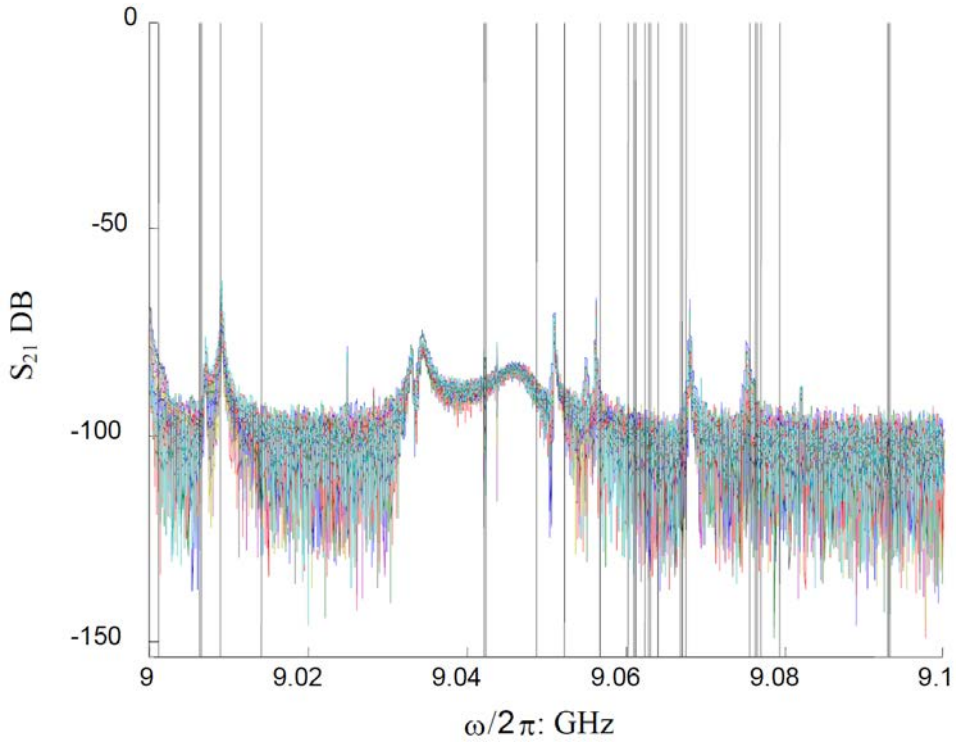

Fig. 15 Comparison of 5th dipole band experimental RSA data (in which beam moved with cross offset – various colours relate to different offsets) to ACE3P eigenvalues (black lines).

The electric field distribution of some of these modes is displayed in Fig. 16. These modes are not entirely localised to one cavity but are beam-pipe modes and exist localised between two cavities, despite this complicating the experimental analysis they still have the potential to be used as HOM BPM's.

The modes that are truly trapped in the 5th dipole band are in the region of 9.06 GHz to 9.065 GHz. These modes are predicted by the numerical simulations and displayed in Fig. 17, but possess low *R/Q* values and do not couple well to the beam. This is confirmed from the experimental measurements in Fig. 15. As such these trapped modes are not ideal for use as HOM BPM's.

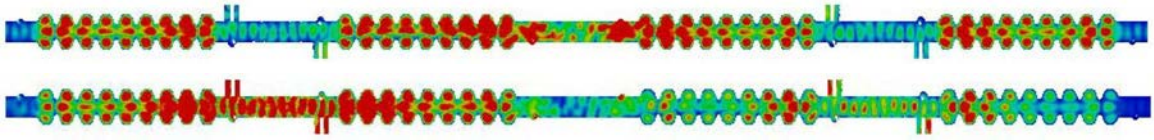

Fig. 16 ACE3P magnitude of the electric field for selected modes from the 5th dipole band: 9.000 GHz (top) and 9.0064 GHz (bottom).

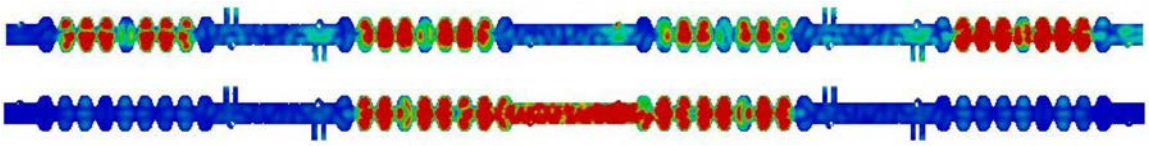

Fig. 17 ACE3P magnitude electric field distributions from the 5th dipole band: 9.061 (top, trapped mode) and 9.062 (bottom, inter-cavity mode).

Earlier simulations, based on single cavities, show significant frequency shifts from the multi-cavity results obtained recently with Omega3P eigenfrequencies. *R/Q* values obtained with Omega3P simulations are shown in Fig. 18. We note that a region with good coupling exists between 7 GHz to 8 GHz. This is a region densely populated with multipoles ranging from monopole up to sextupole modes. Mode identification is not straightforward and will be problematic if used for diagnostic purposes refer to Fig. 19.

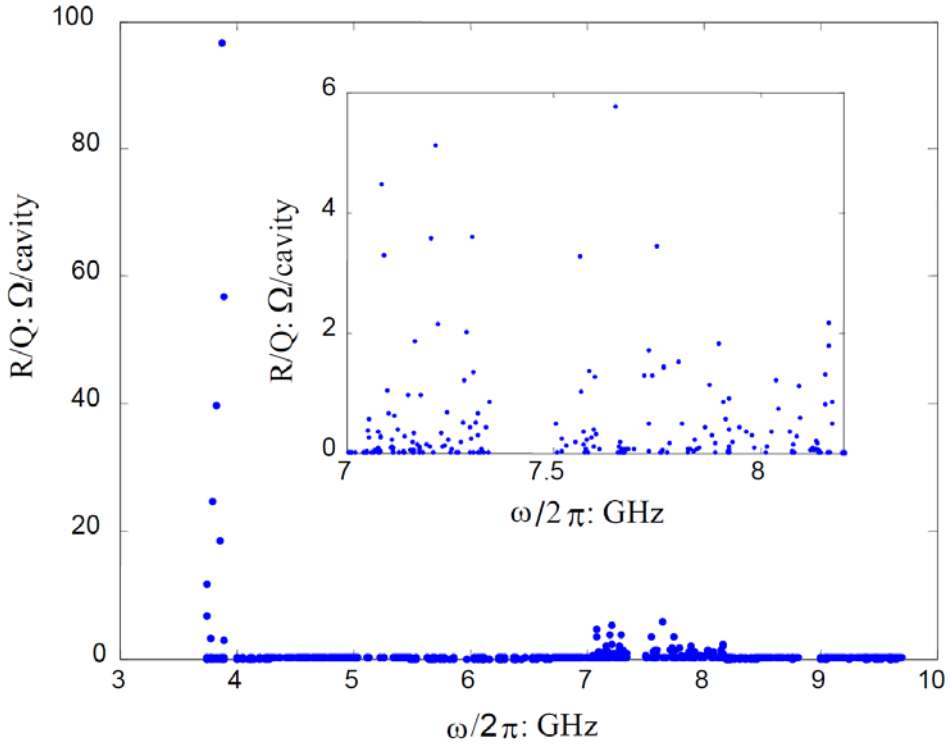

Fig. 18 R/Q values calculated using the Acdtool of ACE3P postprocessor for all modes up 9.8 GHz.

Fig. 19 ACE3P magnitude electric field distributions from the multi-cavity mode at 7.301 GHz.

The first quadrupole band runs from 6.5 GHz to 6.8 GHz, some of these modes are indicated in Fig. 20. This band also contains localised modes. However they are unlikely to be relevant as modes for beam diagnostics.

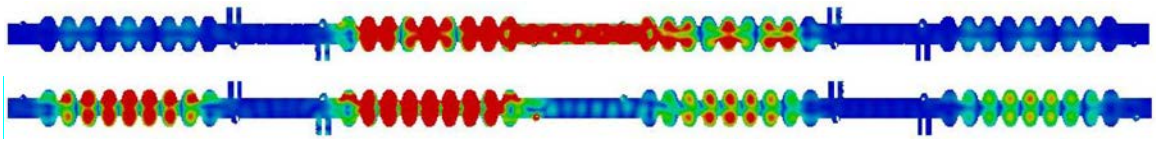

Fig. 20 ACE3P magnitude electric field distributions from the 1st quadrupole band: 6.628 GHz (top) and 6.806 GHz (bottom).

The full eigenmode simulations of the entire ACC39 module, lend an understanding of the modal distributions contained within. This allows for the identification of trapped modes (which would not be observable in the scattering matrix data) and potentially harmful multi-cavity modes as has been demonstrated in this section, in which it is necessary to model ACC39 in its entirety (as compared to the single cavity simulations). However the eigenmode analysis, while useful for the aforementioned reasons, is limited in conveying the actual

amount of energy that is transmitted by any given mode, as would be the case for scattering data. The scattering data provides both the cavity resonances and the power distributed in these resonances. Scattering simulations of ACC39 in its entirety are presented in the following section.

5.2. MODULE BASED SCATTERING SIMULATIONS AND MEASUREMENTS

As mentioned in Section 5.1 the GSM methodology used here is a 2 port calculation, we are unable to calculate the effect of multi-cavity modes measured from the ports of central cavities as this would facilitate a 3 port unit cell calculation. Hence, a comparison with the multi-cavity „N port“ CSC results is possible with this particular GSM method if the full ACC39 cavity string is simulated. All waveguide ports not considered in the GSM calculation are considered as being non-shorted (a magnetic boundary condition is applied at the port). A similar calculation was also made with the S3P driven modal module of ACE3P, with a few exceptions. Firstly the bellows were not considered in the calculation as these proved to be computationally very expensive to simulate. Secondly only a single mode the TEM mode was excited at each port in the S3P calculation. The mesh generated by CUBIT for use with S3P was a third order mesh with more than 3 million elements. The direct comparison of the results obtained from the semi analytical GSM and the numerical S3P method is presented in Fig. 21.

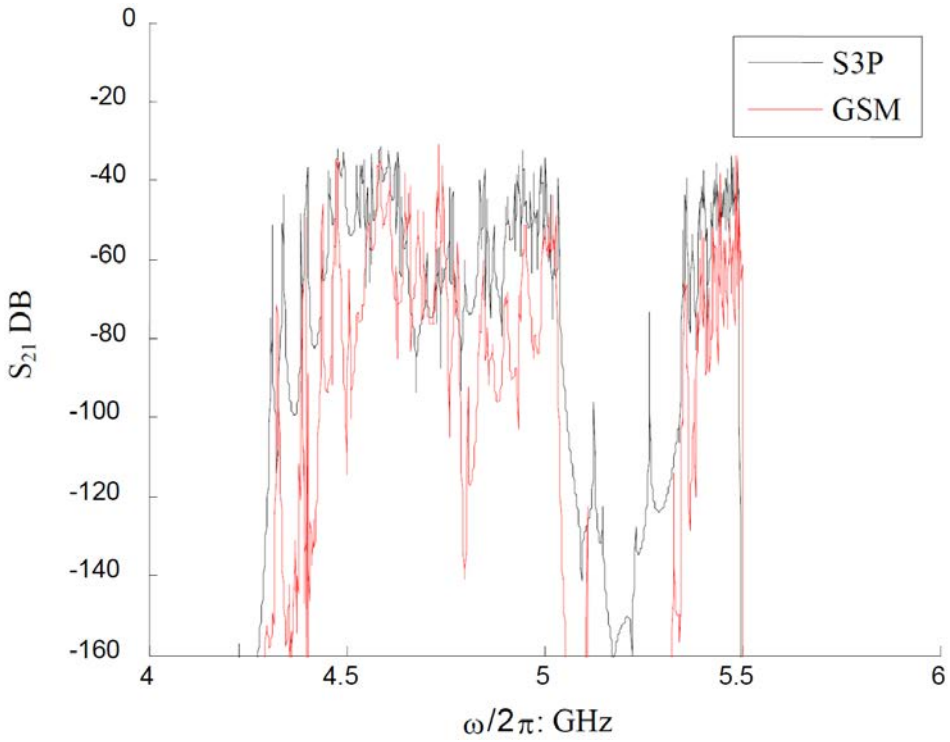

Fig. 21 Comparison of S_{21} calculated by GSM and S3P (ACE3P) across the entire module from the HOM pickup of C1 to the HOM pickup of C4. Note here in this calculation all other ports are bounded by magnetic boundary conditions, so that a direct comparison can be made with the GSM calculation.

It can be seen that GSM gives comparable results to that of the fully simulated structure. However below 4.39 GHz the agreement wanes. We attribute the discrepancy in the results as being due to modes below cut-off (the beam-pipe cut-off is ~4.39 GHz for dipole modes) in the cascaded blocks. The method relies on there being at least one propagating mode present

in order to be accurate. This is further emphasised by GSM calculations conducted with less modes, where this discrepancy in the region of the cut-off becomes more noticeable.

A full analysis of all the passbands consisting of a 9cell ACC39 structure up to 10GHz have been previously investigated and published in: “Compendium of Eigenmodes in Third Harmonic Cavities for FLASH and the XFEL," DESY Report: DESY 12-053, 2012” in which the first dipole frequency band is between 4.30GHz and 4.93GHz, the second is 5.35GHz to 5.50GHz, the third is from 6.82GHz to 7.62GHz, the fourth is between 8.50GHz to 8.92GHz and the fifth is from 9.05GHz to 9.09GHz. Note other HOM’s are inter-dispersed after the second dipole band.

In order to understand the complexities of the multi-cavity modes in ACC39 we utilise the S3P suite of ACE3P to forego the limitations imposed upon GSM both by the maximum number of port modes in HFSS (of 25 modes per port) and the 2 port restrictions of the methodology. We first consider the propagation of power throughout the entire module by looking at the transmission from the first downstream HOM coupler (P1) of cavity C1 into each subsequent HOM coupler upstream. In this S3P calculation we consider all of the ports (including the power couplers) in ACC39; no magnetic boundaries are applied at any of the ports. The results of this calculation are displayed in Fig. 22.

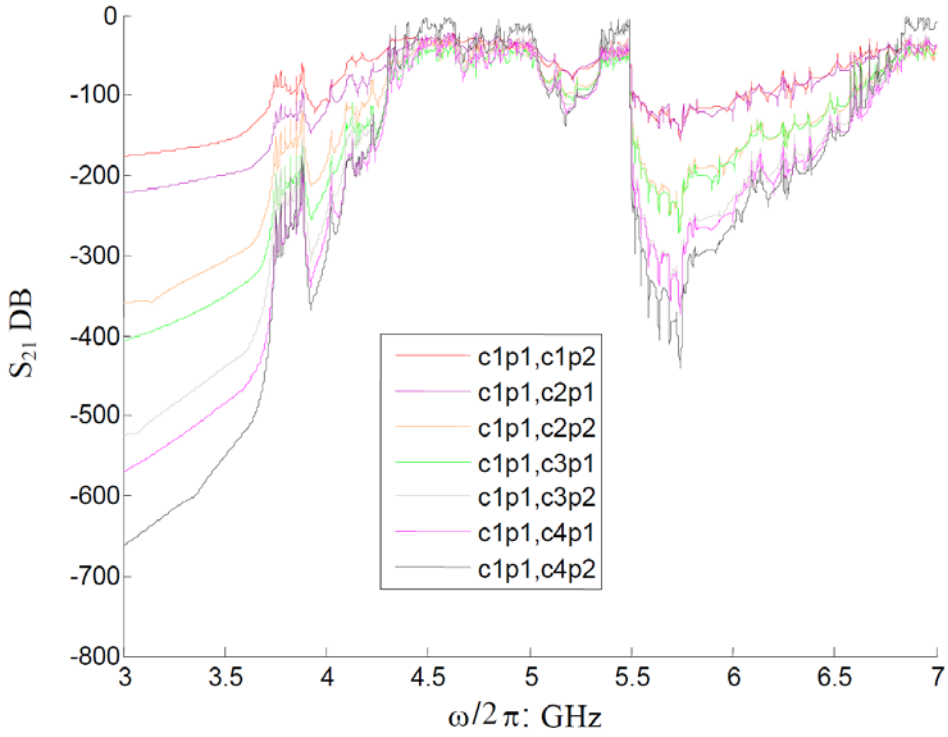

Fig. 22 Comparison of S_{21} transmission data across ACC39 calculated by S3P. Here the transmission from the first HOM pickup of cavity C1 (c1p1) is tracked throughout the entire module of ACC39 at each subsequent HOM pickup (c1p2 to c4p2).

From Fig. 22 we clearly observe the loss in power as the modes propagate down the module particularly in bands that do not propagate across cavities such as the first monopole band, the first beampipe band, the region just after the second dipole band and before the first quadrupole band. We also note stronger coupling between the transmission from a p1 coupler to a p2 coupler in the multi-cavity regions.

Next the effect of looking at the transmission across each subsequent cavity individually in the string was investigated. In these S3P calculations we consider all of the ports (including the power couplers) in ACC39; no magnetic boundaries are applied at any of the ports. The transmission from the downstream HOM coupler p1 and the upstream HOM coupler p2 for each individual cavity (C1 to C4) was made as a series of separate calculations in which the power is transmitted from p1 to p2. The results from the first cavity C1 and the last cavity C4 calculations are compared in Fig. 23. All the calculations across the individual cavities in ACC39 produced different frequency spectra; no two cavities had directly comparable results. This is a disturbing development, as it suggests that the multi-cavity nature of ACC39 does not amend itself to readily identifiable modes that can be used for a HOM BPM system, since within each cavity the eigenfrequencies will be different.

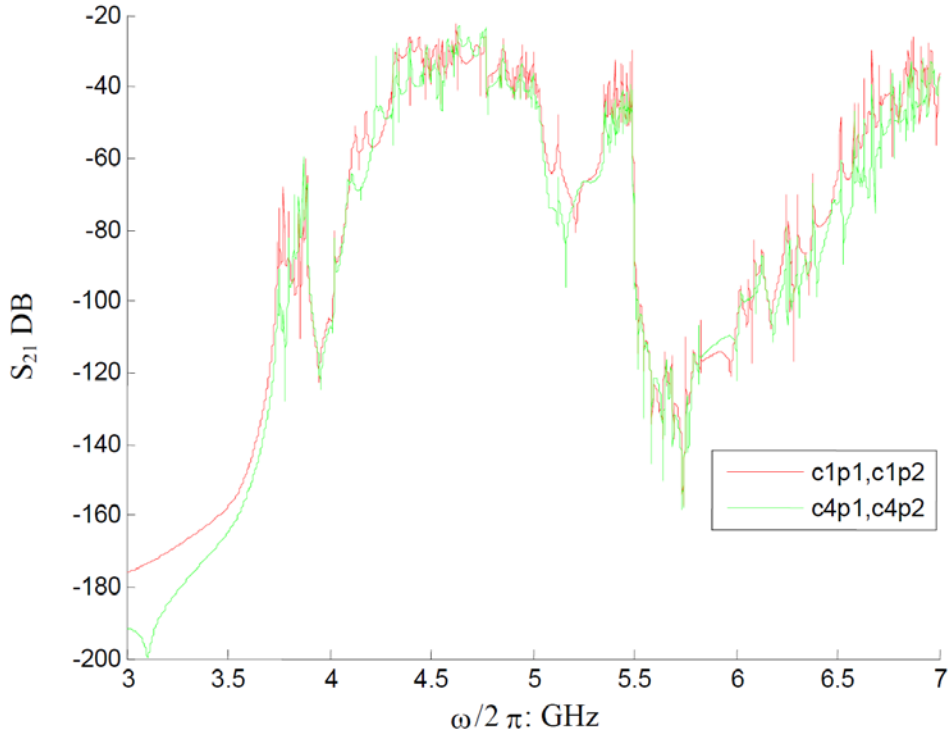

Fig. 23 Comparison of S_{21} transmission data across ACC39 calculated by S3P across individual cavities. Here we compare the transmission across the first cavity C1 (c1p,c1p2) to that of the last cavity C4 (c4p1,c4p2), in which the individual transmission from the downstream (p1) to upstream (p2) HOM couplers is considered as separate calculations.

As a check that these results are due to the multi-cavity modes and are not an artefact of the numerical calculations we made further calculations using S3P in which we considered the beampipe modes. The results of these calculations are displayed in Fig. 24. From Fig. 24 we note that c1p2,c2p1 and c3p2,c4p1 give identical results, we would expect this as these two beampipe sections have the same geometry and the beampipe modes are not multi-cavity in nature. We expect the results from c2p2,c3p1 to differ since this section has a different geometry to that of the other beampipe sections (due to the coupler arrangement). This calculation reaffirms that our calculations are physical.

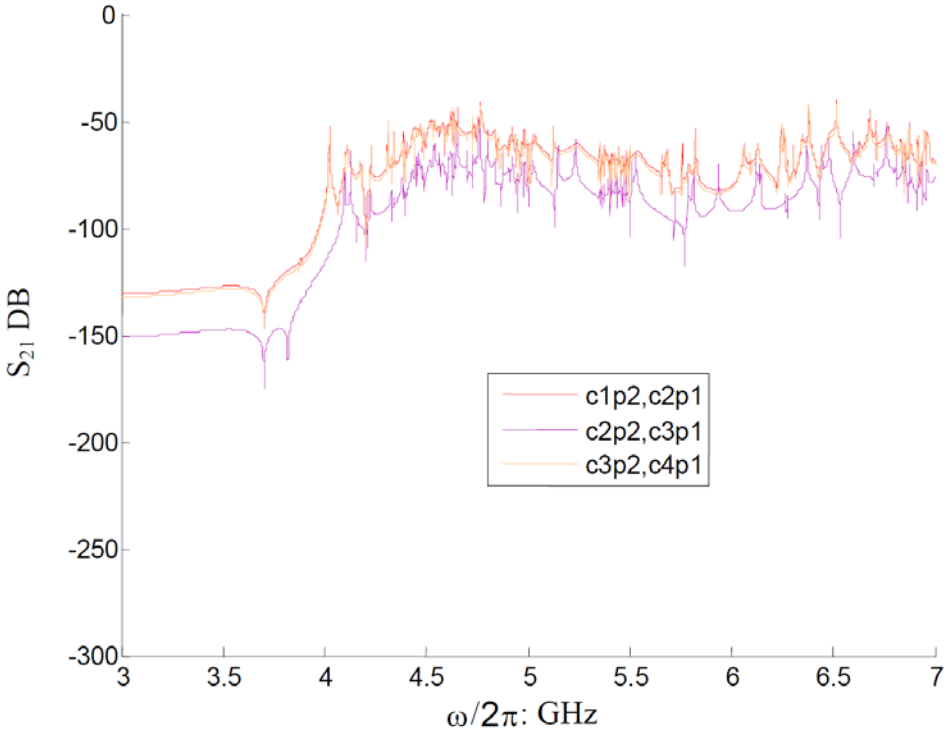

Fig. 24 Comparison of S_{21} transmission data across ACC39 calculated by S3P across the individual beampipe sections. Here we compare the transmission across the beampipe sections (c1p2,c2p1), (c2p2,c3p1) and (c3p2,c4p1) in which the individual transmission from the downstream (p2) to upstream (p1) of the respective HOM couplers is considered as a series of separate calculations.

In the following section we compare the results of this theoretical investigation to those from the experiments conducted with ACC39 installed at FLASH, DESY.

5.3. COMPARISON OF MODULE BASED SIMULATIONS TO MEASUREMENTS BASED ON THE GSM SCATTERING PARAMETER RESULTS

While there is reasonable agreement between the calculations made using GSM and S3P for an idealised ACC39 structure, when compared to the experimental data in which there was no beam present we observe a qualitative agreement, as seen from Fig. 25, and note a few regions where there are large discrepancies: from 4.4 GHz to 4.6 GHz and 6.6 GHz to 7 GHz. This may indicate both coupling of cavity modes and frequency shifts due to fabrication errors as departures from the idealised structure used in the simulations. If we consider a single region such as the 5th dipole band when a comparison is made across a single cavity between the theoretical idealized results and those obtained from the experimental data, such as that displayed in Fig. 26.

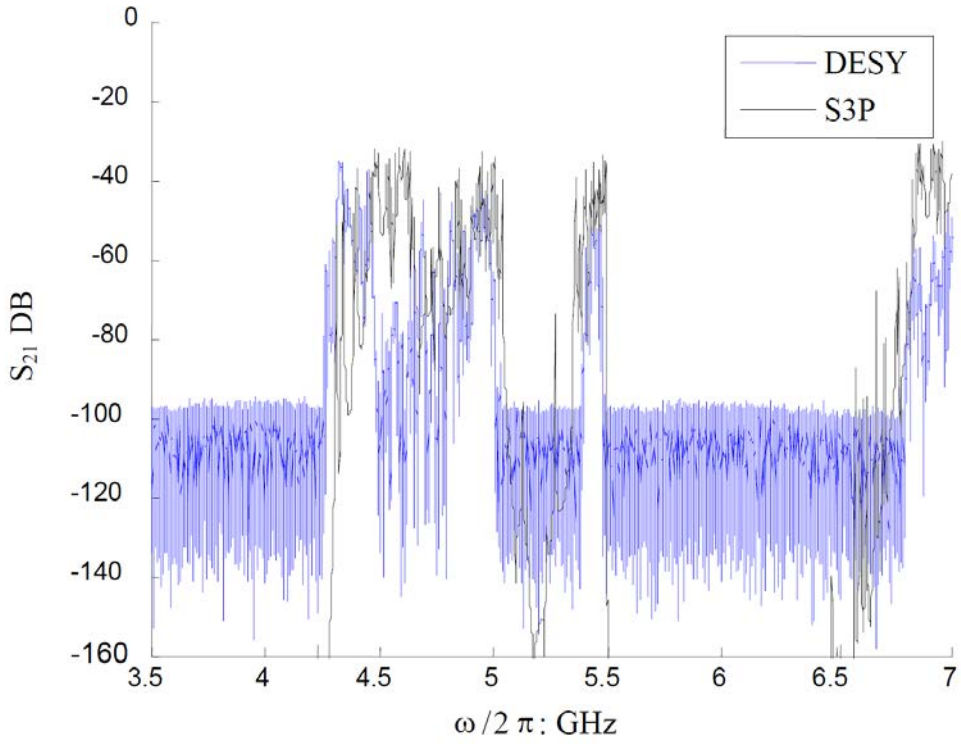

Fig. 25 Direct comparison of calculated S_{21} (S3P) and the experimental data (DESY) taken across the entire ACC39 string for transmission from C1, upstream HOM-coupler, to C4, downstream HOM-coupler.

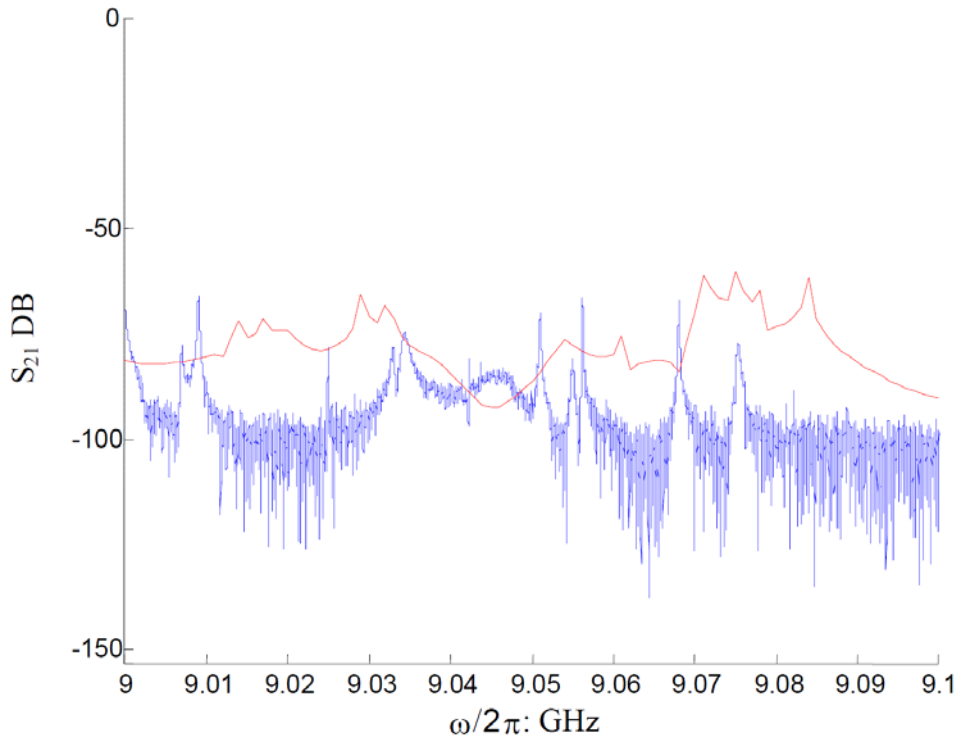

Fig. 26 Direct comparison of the 5th dipole band calculated S_{21} (S3P in red) and the experimental data (DESY in blue) taken across cavity C2 ACC39 string for transmission from the downstream HOM coupler p1 to the upstream HOM coupler p2. Here the black dashed lines are the eigenmodes calculated previously using OMEGA3P. Note the OMEGA3P and the S3P calculations used a different set of boundary conditions (refer to the appropriate sections regarding these details).

Certain similarities can be observed between the experimental and the idealized scattering matrix data. The similar peak structure however appears to be shifted in the order of about 10 MHz, we still observe splitting of most of the recognizable peaks, but the agreement is far from adequate. We also note a discrepancy between the eigenmode calculations form OMEGA3P and those from S3P; however we attribute these to the different boundary conditions used in their calculations. To further illustrate the discrepancy between the idealised theoretical calculations and the experimental data consider the comparison of the transmission across cavity C4 in the ACC39 module which is displayed below in Fig. 27.

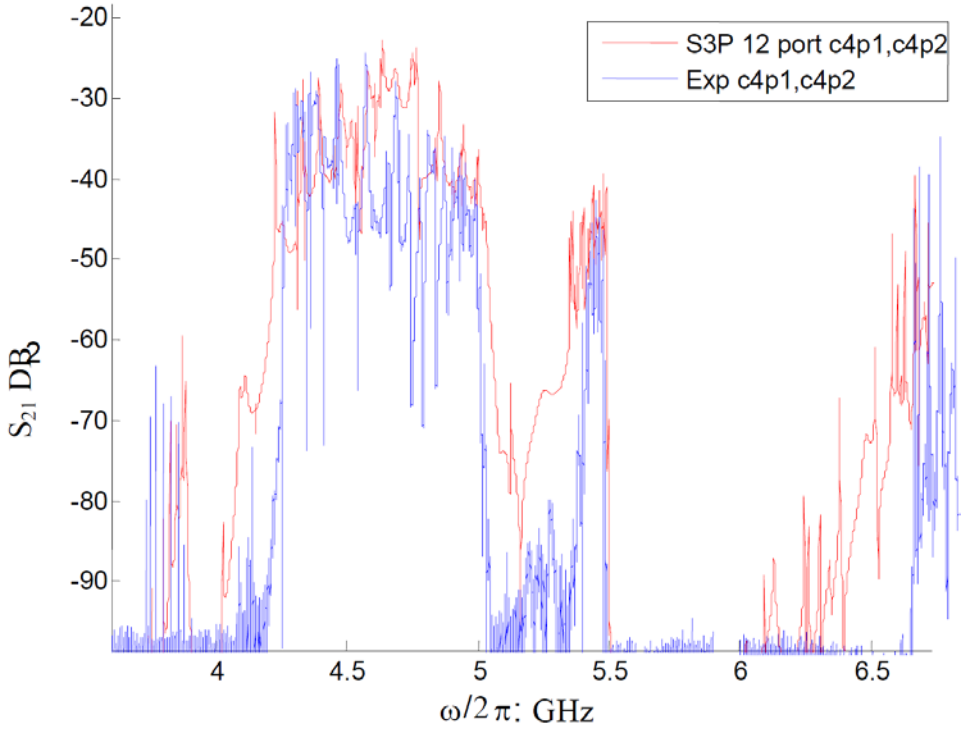

Fig. 27 Direct comparison of calculated S_{21} (S3P in red) and the experimental data (DESY in blue) taken across cavity C4 ACC39 string for transmission from the downstream HOM coupler p1 to the upstream HOM coupler p2.

While the passband structure is easily discernible from either the theoretical or experimental data in Fig. 27, there is clear disagreement between that predicted and what is measured, particularly in the 2nd dipole band, the 1st beampipe band. These discrepancies may be the result of misalignments or machining defects in the structures which have the effect of shifting the multi-cavity HOMs en-masse. This aspect, the sensitivity of multi-cavity HOMs in ACC39 is investigated in the next section as a means to explain and understand these discrepancies.

5.4. COMPARISON OF MODULE BASED SIMULATIONS TO MEASUREMENTS BASED ON THE CSC SCATTERING PARAMETER RESULTS

This section presents the comparison between measured and S-parameters simulated by the CSC technique in combination with the Fast Resonant Solver of CST MWS. Fig. 28 shows the measured (blue) and simulated (red) absolute transmission spectrum through cavity 3. The noise floor of the measured transmission spectra is observable at -100 dB. The nine sharp peaks of the fundamental TM monopole passband are visible in the interval from 3.72 GHz to 3.92 GHz. The first two TE dipole passbands are reflected in both curves in the interval from 4.25 GHz to 5.50 GHz. In the range from 5.50 GHz to 6.55 GHz a stopband is located. Based on the previously performed eigenmode computations, the peaks in the interval 6.55 GHz to 6.8 GHz are assumed to belong the quadrupole passband. The bandpass above 6.8 GHz shows the excitation of modes of the second TM monopole passband.

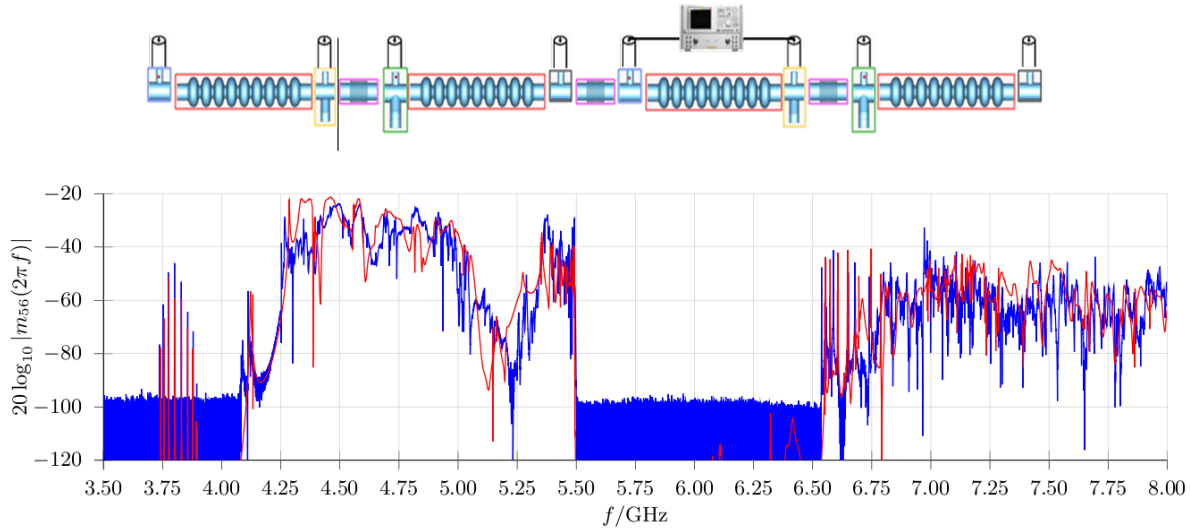

Fig. 28 Comparison between the absolute value of the transmission through cavity 3. The red curve shows the numerically determined transmission spectra, whereas the blue curve plots the measured data.

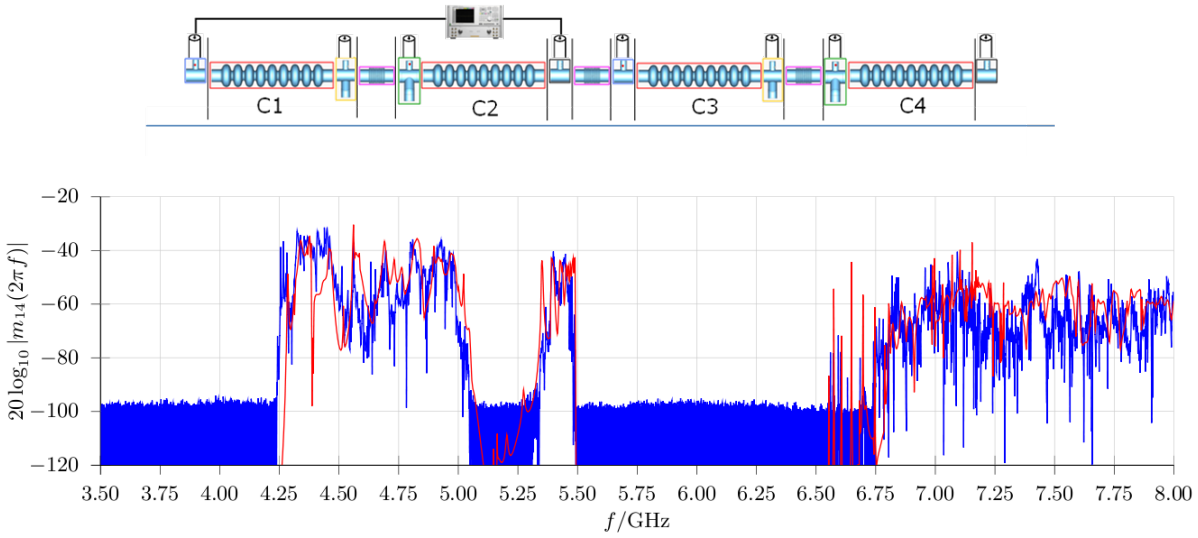

Fig. 29 Absolute value of transmission spectra via cavity 1 and cavity 2 (i.e. transmission from coupler C1H2 to C2H2). Blue shows the measured spectrum and red the simulated. The fundamental passband is not observable in the spectra because the frequencies of the respective peaks are below the fundamental cutoff frequency of the beam pipe connecting the adjacent cavities via the bellows.

Fig. 29 depicts the transmission via cavity 1 and cavity 2. In comparison to the transmissions through single cavities in the chain, the fundamental passband is not visible in the measured and simulated spectrum. As the cutoff frequency of fundamental waveguide mode in the beam pipe is larger than the resonant frequencies of modes in the fundamental passband, the fundamental passband is confined to the individual cavities. Consequently, these modes do not couple across different cavities. However, Fig. 29 conveys that higher order modes (such as the first and second dipole passband, the first quadrupole passband or the second monopole passband) are able to couple across the cavities via the bellows (inter-cavity modes).

Fig. 30 shows the transmission via the entire cavity chain. Similar as in Fig. 29 peaks of the fundamental passband are not in the spectrum, but peaks corresponding to HOMs coupling

across the chain are observable. However, in contrast to the measured curve (blue), the simulated curve (red) shows resonances attributed to quadrupole modes.

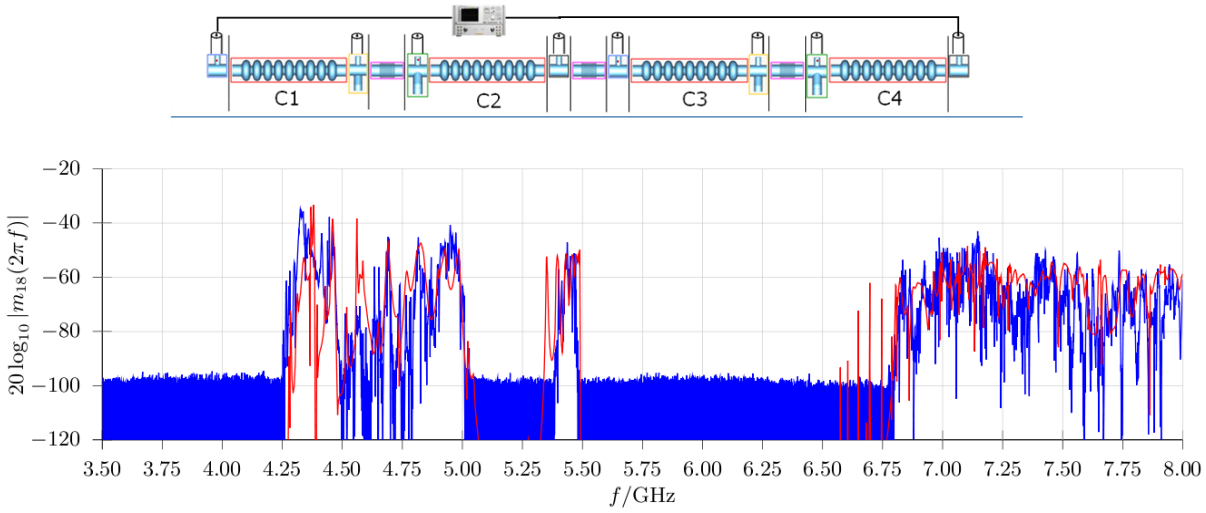

Fig. 30 Absolute value of transmission spectra via the entire cavity chain. In accordance to the previous figure, the fundamental passband is also not observable in the spectra because the frequencies of the respective peaks are below the fundamental cutoff frequency of the beam pipe connecting the adjacent cavities via the bellows.

All plots presented here have in common that the agreement between measurement and simulation is by far not perfect. However, the principal physical properties of the ACC39 string are reflected by the computer model in a very reasonable way. For instance, the locations of the pass- and stopbands agree in a very good manner. Moreover, distinct peaks in the e.g. fundamental and quadrupole bands coincide remarkable. The observed differences between measurement and simulation are attributed to the following not yet considered effects in the computer model.

1. Deviations of the cavities from their ideal shape due to fabrication tolerances, different mechanical histories, tuning and cool down processes.
2. Frequency dependent reflections from the HOM- and input couplers due to the connected waveguide feeding and absorbing system.
3. Interactions of the ACC39 cavity string with other devices in the beamline, e.g. the bunch compressor (downstream) or ACC1 (upstream). Although not presented in this report, the transmission coefficient from the upstream HOM coupler of cavity 1 at ACC39 to the closest HOM coupler in ACC1 (module next to ACC39) has been taken. The spectrum shows that coupling between ACC1 and ACC39 takes places. Consequently, presented measured properties of ACC39 also depend on e.g. ACC1.

6. SENSITIVITY OF ACC39 HOM SPECTRUM TO ALIGNMENT AND FABRICATION ERRORS

Fudicial work on the sensitivity of the first monopole band to fabrication errors was conducted using a circuit model and mode matching approach. The results of this investigation are detailed here, this initial work considered only a single cavity sans couplers isolated not contained within the ACC39 module (i.e. the effect of multi-cavity HOMs was not considered) and only investigated the monopole bands, in particular the fundamental band. It was found that the fundamental band of ACC39 was quite sensitive to fabrication errors as

can be seen in Fig. 31. In Fig. 31(a) we observe the sensitivity of a single middle cell of ACC39 to variation in geometric factors for the fundamental mode in which this mode is tracked in terms of fixed periodic boundaries; this calculation was made using the mode matching. In Fig. 31(b) the sensitivity of a single cavity for the first monopole band between an idealised perfect structure (sans couplers) and the RMS of 20 different simulations in which the geometric factors of each cell were randomly varied within a tolerance of ±100 μm, note this calculation was also made using the mode matching technique. These calculations show that ACC39 is sensitive to fabrication and alignment errors; however we naturally wish to extend the calculations to include the effects of the sensitivity on the multi-cavity HOMs. It would be computationally very expensive to randomly add errors to ACC39 using S3P to obtain an RMS value in terms of the sensitivity. Instead we utilise the GSM methodology from Section 4.1 as it has been established in the previous sections that this technique is both rapid and accurate. Here we simulate random errors in the ACC39 structure by adding small pipe sections of random length to the existing GSM unit cell. These pipe sections of random length are calculated analytically, these sections serve the purpose of randomly shifting the concatenated scattering matrices in a similar manner as what would occur if a geometric error was included in the GSM unit cell calculations. By adding these pipe sections of random length to all the GSM unit cells within the overall GSM calculation it is possible to explore the sensitivity of the entire ACC39 module in terms of the effect on the multi-cavity HOMs with the structure.

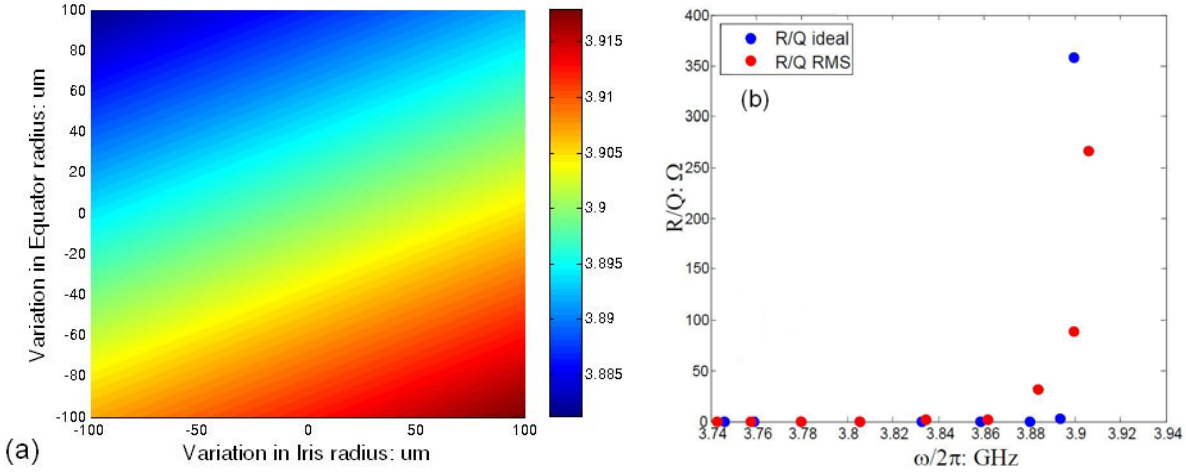

Fig. 31 (a) Contour plot of the sensitivity of a single middle cell of ACC39(for fixed periodic boundaries) to variations in geometric factors. (b) Comparison of the first monopole band between an idealised perfect structure (sans couplers) and the RMS of 20 different simulations in which the geometric factors of each cell were randomly varied within a tolerance of ±100 μm.

The RMS of 30 separate calculations with random seeds is displayed in Fig. 32, in these calculations the length of the random pipe sections was varied with an RMS of 0.35 mm. In this figure we clearly observe that ACC39 is very sensitive to such errors and what we observe in Fig. 32 is similar to what we observe in Fig. 26 and Fig. 27 in terms of the large discrepancies.

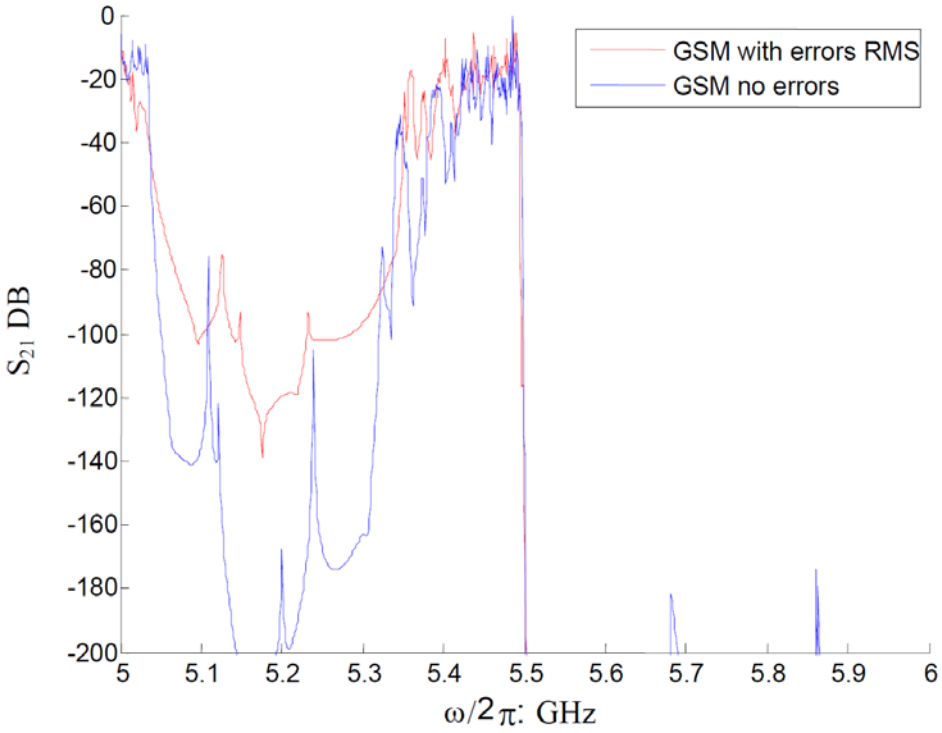

Fig. 32 S_{21} calculated by GSM using 20 modes per port across the entire module of ACC39 (c1p1,c4p2). Note here in this calculation all other ports are bounded by magnetic boundary conditions. Here we compare the idealised GSM calculation (blue) to that of the RMS of 30 GSM calculations (red) in which random errors with an RMS of 0.35 mm have been added throughout ACC39 module.

We would note that in the case of the beampipe modes, although they are localised within ACC39 the bellow sections themselves are by their very nature flexible and would facilitate the shifting of these modes from their calculated idealised positions.

7. MAIN INFLUENCE OF THE LOCATION OF PERTUBATIONS ON HOMS AND TRANSMISSION SPECTRA

Apart from measuring beam parameters based on the HOM port signals, it is desirable to obtain information on the perturbations of the cavity deduced from transmission spectra or HOM port signals. To principally investigate the dependency of the location of a perturbed cell on the transmission spectra of a nine-cell resonator, the third harmonic cavity is again decomposed into mid-cell and end-cell. The scattering parameters of the individual cells are computed by the Fast Resonant Solver of CST MWS. The comparison between direct and element-wise computation is shown in Fig. 33 for the sake of validation. The cyan curve depicts the transmission through the cavity related to the TE_{11} port mode. The magenta line shows the transmission obtained by the CSC approach. Both curves show a good agreement. The resonances observed at 3.9 GHz in the cyan curve are attributed to the fundamental monopol passband. This passband only couples in an artificial manner to the TE_{11} dipole modes, due to the rotational symmetry of the structure. In a next step, the scattering parameters of a perturbed mid-cell are computed. The perturbed cell has a cup length 18.2167 mm instead of 19.2167 mm.

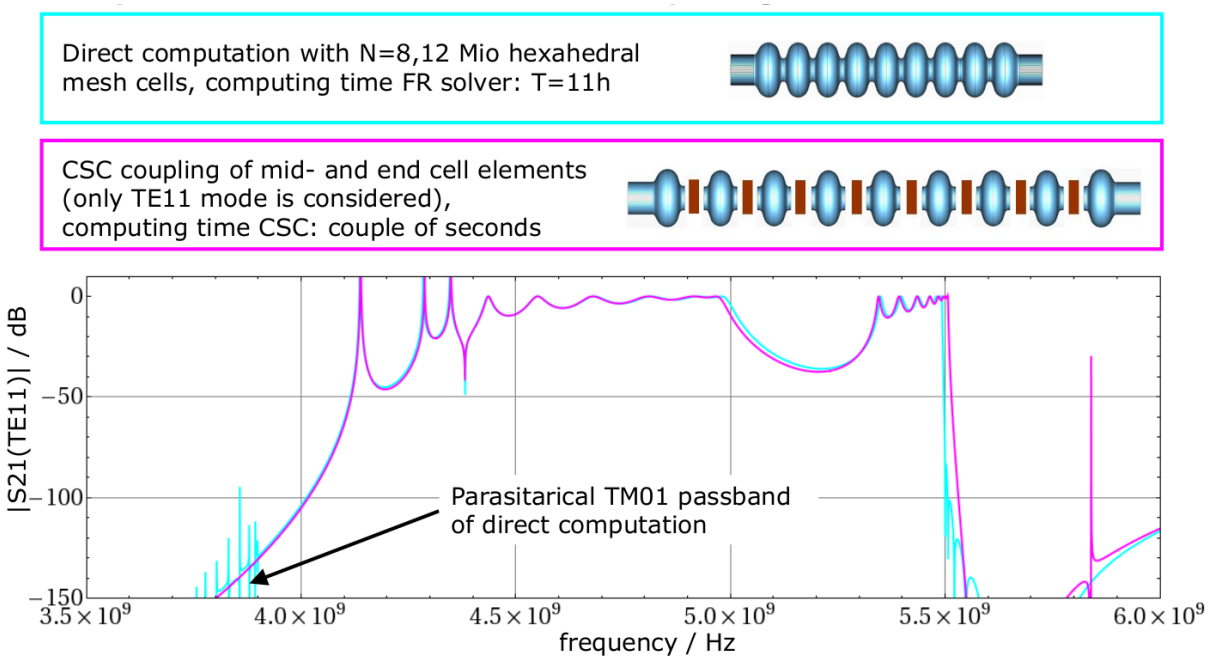

Fig. 33 Transmission through a third harmonic cavity without couplers. The cyan curve shows the spectrum computed by means of full discretization of the cavity, whereas the magenta curve shows the spectrum computed by the CSC method.

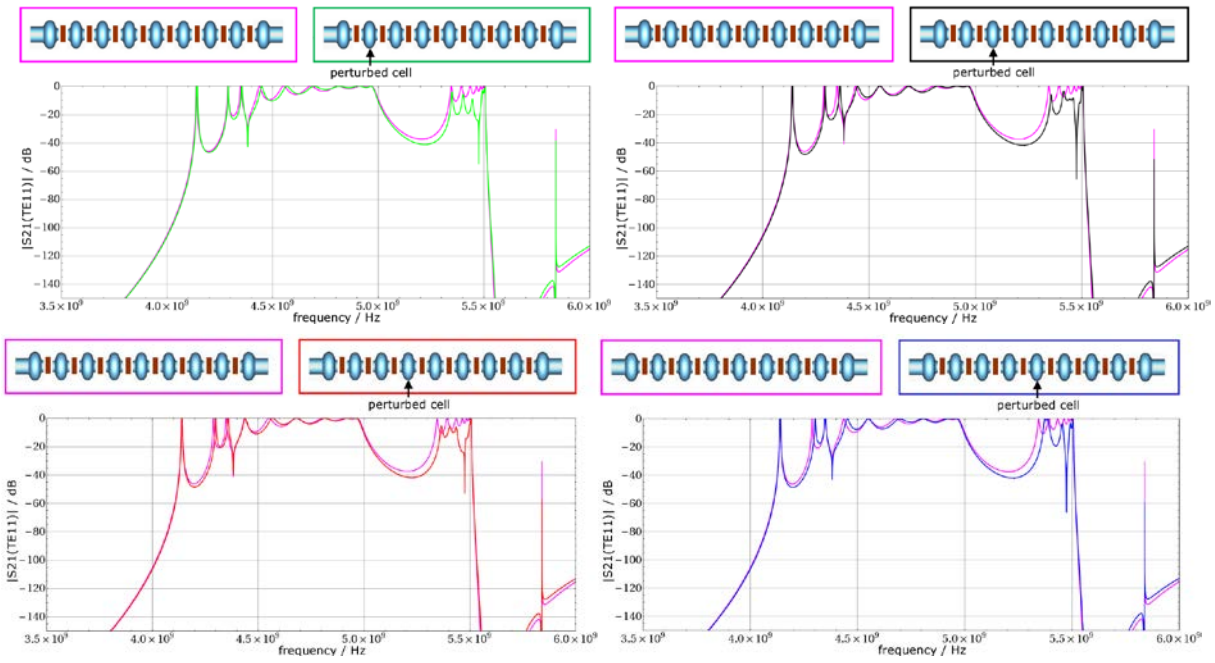

Fig. 34 Transmission spectra in dependency on the location of the perturbed cell. The perturbed cell is created by shrinking the cup length of the mid-cell from 19.2167 mm to 18.2176 mm. As the cavity is a symmetric rf device, the spectra arising by locating the perturbed cell at the positions 5 - 8 are not shown (the curves are equal to the curves depicted above).

The perturbed cell is mounted in the nine cell resonator at different positions and the transmission spectra are computed by means of CSC (see. Fig. 34). In contrast to the first dipole passband, the second dipole passband is very sensitive to the position of the perturbed cell. Moreover, no straightforward mechanism to allocate the perturbed cell in the chain based on HOM spectrum is observable. This suggests that machine diagnostics based on HOMs is a very difficult task.

8. BEAM POSITIONS FROM DIODE DOWN MIXED HOM-SIGNALS - EVALUATION SCHEMES

The following work was supported by the German Federal Ministry of Education and Research (BMBF) under contract 05K10HRC and in parts by the EU-FP7 EuCARD program, it is presented here due to its close ties with the ACC39 work package program.

The excitation of wake fields in accelerator cavities by the beam is an unavoidable effect, which may lead to harmful consequences concerning cooling demands and beam quality. Therefore many cavity designs include specific Higher Order Mode (HOM-) couplers intended to lead beam deposited fields out of the cavity. It is common practice to terminate these couplers externally with resistive loads in order to dump the beam-excited high frequency signals. Research of the past decade demonstrated the possibility also to deduce beam properties, mainly the transverse beam position, from HOM coupler signals, trying to avoid the need of beam position monitors. Typically this is done with dedicated electronic hardware that replaces the terminating dumps. It filters out all but those signal components from two distinct orthogonal dipole mode polarisations. Modes of dipole type are preferred since some of them interact strongly with the beam and since their signal amplitude depends (in good approximation) linearly on the beam's distance to the cavity's axis of rotational symmetry. This implies the need of well-tuned narrow band filters, down-mixing stages including a local oscillator and mixers and, for final read-out, analog-digital-converters.

8.1. THE CONCEPT

Starting from the idea to avoid the need of a local oscillator we investigate the possibility to replace most of the specific hardware listed above by a broadband radio frequency detector diode like it is illustrated in Fig. 35. This diode is intended to operate as a mixing instance that produces a low-frequency signal by combining at least two, but typically a large set of spectral lines of the HOM-coupler signal. Since different polarisations of fields are to be expected at slightly different original frequencies (which is a consequence of the non-ideal rotational symmetry of the cavity) their contributions should appear at different places in the down-mixed spectrum. If furthermore both polarisations have a non-vanishing coupling to the HOM-coupler under consideration the down-mixed signal is therefore expected to carry information about the beam-position in both transversal coordinates. Abandoning the primary narrow-band filters obviously will lead to a superposition of several high-frequency signals, each associated to a certain mode frequency and decay time. After down-mixing an even more

complicated temporal dependence is to be expected. This demands for an evaluation scheme capable to distinguish dominant contributions in a large set of measurements. We apply the Singular Value Decomposition (SVD-) technique as a black-box solution, implemented e.g. in Mathematica©. The SVD reduces the low-frequency time-domain signal, typically consisting of several thousands of sample points, to a small set – in most cases not more than ten – of amplitudes, but it performs no correlation to any physical parameter. This is done in a second evaluation step. It is one main purpose of this paper to demonstrate that this correlation of SVD-amplitudes of diode down-mixed HOM-signals with the transversal beam coordinates is of linear type.

8.2. EXPERIMENTAL SETUP AND PROCEDURE

Following the description above we connected AGILENT 423B detector diodes with the HOM couplers of DESY-FLASH modules ACC1 (some) and ACC39 (all), as shown in Fig. 35.

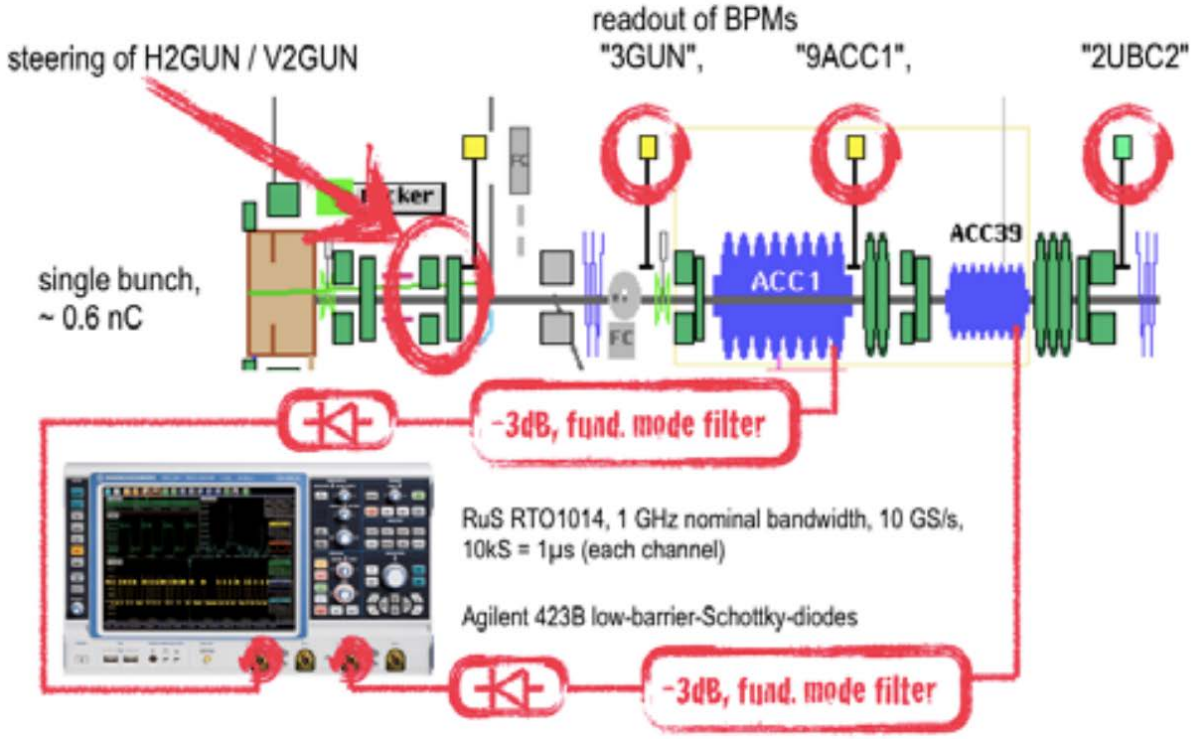

Figure 35: Main experimental components. Sketch of FLASH setup taken from DOOCS [7] display. Signals taken from the HOM-couplers (multiplexing switch not shown) are filtered to suppress fundamental mode components, down-mixed in the RF detector diodes and sampled using a standard oscilloscope.

This was done at a switchboard neighbouring to the accelerator using the firmly installed cable connections. These cables introduce a signal damping of -10 dB … -15 dB. Coaxial 3dB attenuators were used mainly in order to protect the diodes against potential electrostatic charging (even though there was no evidence for such). As matter of experimental experience additional filters were needed in order to suppress the 1.3 GHz-/3.9 GHz-fundamental mode

signal, which dominates the HOM-coupler signal in spite of the coupler's own fundamental mode notch filters. At ACC1 MiniCircuits VBF-1575+ band passes were used, which have their main transmission close to the frequency range of the first dipole mode passband. For ACC39 high pass filters MiniCircuits VHF-4600+ demonstrated to be well suited. Unlike ACC1 (and all other accelerating modules of FLASH) with several clearly cavity-localised HOMs the cavities of module ACC39 are strongly coupled through the beam pipe for almost all HOMs. This typically reduces the beam-mode interaction and makes the identification of modes, which are well suited for individual detection, a difficult task. Therefore we experimentally tried to feed at ACC39 a HOM spectrum with a very wide range into the diode. Signal detection and data storage was performed using a Rohde & Schwarz RTO1014 oscilloscope. In comparison with other brands it turned out that a 10 GS/s sampling rate and a best sensitivity of 1mV/div with a digitising step of ~ 40 μV were important assets in this application (if multibunch operation also is intended, a memory depth sufficiently large to capture one entire bunch train (e.g. 400 μs × 10 GS/s = 4 MS) is needed). Triggering of the oscilloscope was performed without external source, directly using the diode signal. When operating simultaneously on both modules ACC1 and ACC39 the signal of the former was used. Different vertical offsets of the beam, which was accelerated in ACC1, were achieved by adjusting two steering magnets. For each setting the measurements of three beam position monitors (BPM) of FLASH were read out from the DOOCS system and saved together with the down mixed HOM signals. In one series of 25 measurements signals from ACC1, cavity 8, HOM coupler 1 and ACC39, cavity 4, HOM coupler 2 were observed simultaneously. In a second set of 31 measurements the signals of all 8 HOM couplers of ACC39 were captured sequentially with a single diode, using an additional multiplexing switch.

8.3. EXPERIMENTAL DIODE RESULTS FROM ACC39

Taking an entire ensemble of Ns down-mixed signals (Fig. 36, there Ns =25) as input for a SVD procedure results first in a set of dominant signal forms ("SVD vectors", Fig. 37).

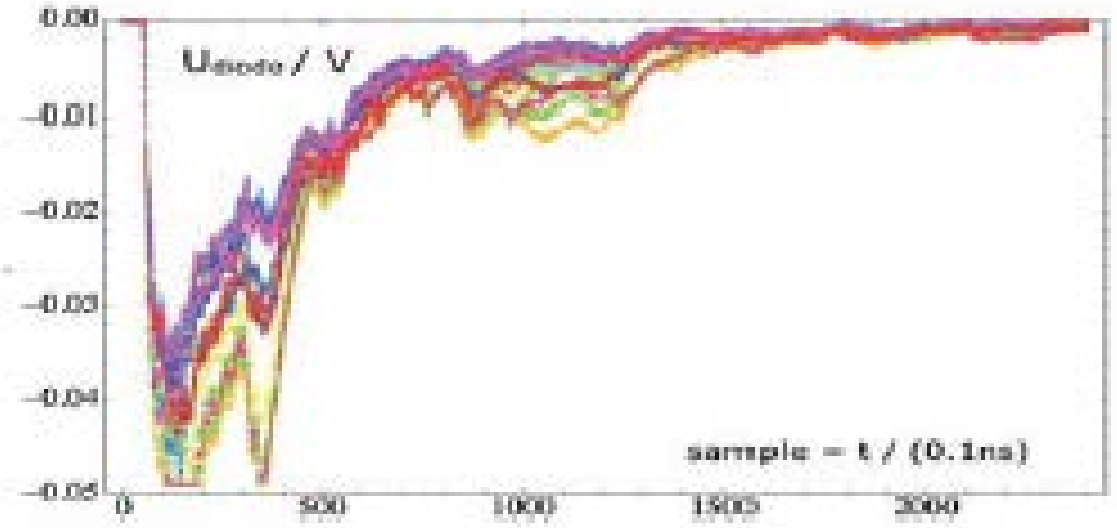

Figure 36: Set of 25 diode down-mixed signals from ACC39, cav. 4, co. 2, each belonging to a steerer setting.

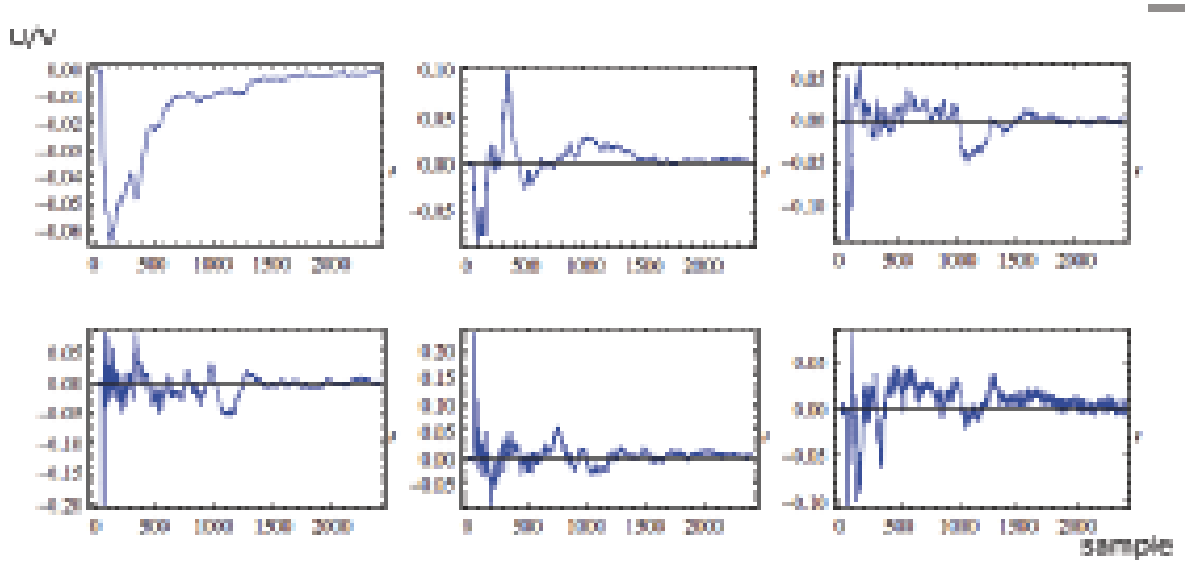

Figure 37: Dominant 6 signal forms of the set of Fig. 36.

Further the SVD determines a matrix of the weights of all SVD vectors in all signals. Let **U** be a submatrix of it, taking only a reduced set of the first Nv most dominant vectors, thus **U** being of dimension Ns × Nv. Fig. 37 illustrates that often very few vectors (there Nv = 4) are sufficient to reconstruct the raw signals very well.

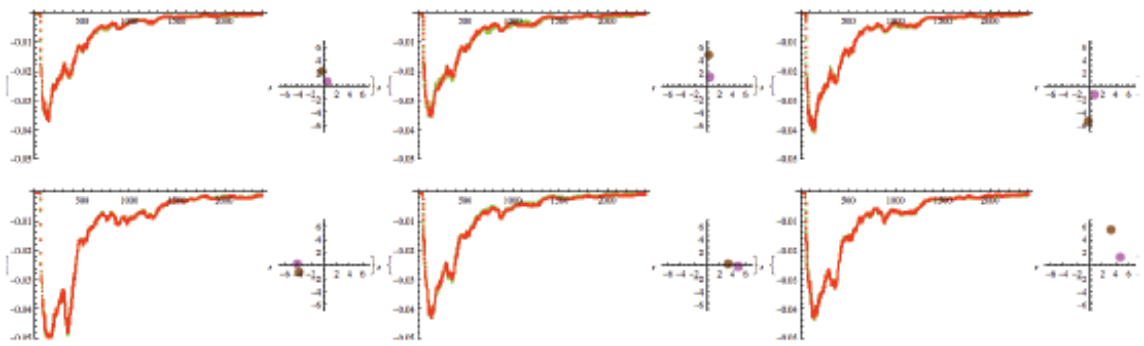

Figure 38: Reconstruction of six freely chosen original signals from Fig. 37 (green, mostly hidden) using the superposition of the first four SVD vectors, together with BPM read outs (in mm, magenta "2UBC2", brown "9ACC1").

Let M denote the matrix of BPM read outs, containing x- and y-measurements in front and behind the module under consideration ("3GUN" and "9ACC1" in case of ACC1, "9ACC1" and "2UBC2" for ACC39). M contains in its four columns four values for each steerer setting and therefore is of dimension Ns × 4. In order to find a correlation between the SVD weights U and the physical parameters M, a linear dependence is assumed, which is expressed as a Nv × 4 - matrix S. Then the correlation would read like

$$M = U \cdot S \tag{11}$$

This can be understood as a group of four (since both M and S have four columns) overdetermined matrix-vector equations, which have a well-known best solution (using a least-square norm):

$$S = \left(U^{\mathrm{T}} \cdot U\right)^{-1} \cdot U^{\mathrm{T}} \cdot M \tag{12}$$

Once S is computed the comparison of both sides of (11), i.e. the predicted and the measured BPM read outs, will show how well the assumption of linearity is justified, and how many SVD vectors are needed (see Figures 39a, b).

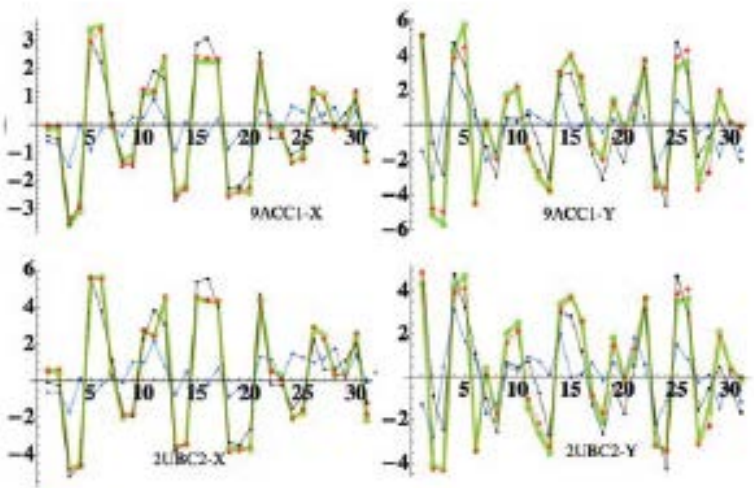

Figure 39a: Comparison of measured (green) and reconstructed BPM read outs in mm for a set of 31 experiments (index as x-value). Signals were taken from ACC39, cav. 4, coup. 2. Blue corresponds to 5, black to 7 and red to 10 SVD vectors used for reconstruction. Whereas the latter reaches very good coincidence in almost all points the first fails totally.

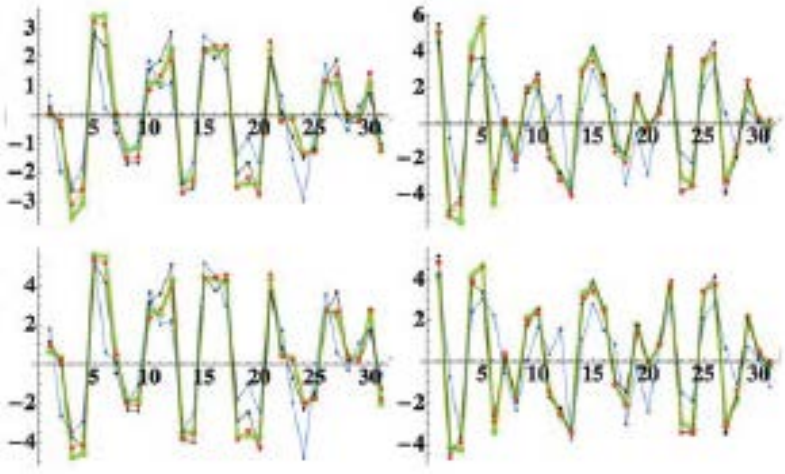

Figure 39b: Like 39a, but signals taken at ACC39, cav. 3,coup. 1. Here reconstruction even with 5 SVD vectors show some poor correlation to the reference, much better with 7 and again best with 10 vectors. This illustrates that the quality of reconstruction in principle depends on the properties and location of the coupler.

8.4. DIODE DOWN-MIXING DISCUSSION

The capturing of HOM signals using an unspecific diode detector was successfully demonstrated. This especially holds for the FLASH-ACC39-module in spite of its strong cavity-cavity coupling and its lack of well distinguishable spectral components. Applying the SVD procedure in combination with a linear regression demonstrates that the assumption of a linear correlation between SVD vector amplitudes and beam position coordinates is well justified. The number of SVD vectors needed is significantly higher than 4, indicating that more physical parameters besides the transversal beam position and momentum are hidden. Furthermore it is remarkable that information about both transversal coordinates can be extracted from a single HOM coupler, even not in the same quality at all couplers of a module.

9. SUMMARY AND CONCLUSIONS

We have investigated the HOM spectrum of ACC39 with the primary purpose of understanding the HOMs in order to identify suitable regions for a HOM BPM system. Previous eigenmode calculations using an idealised cavity without couplers highlighted both the 1st beampipe and the 5th dipole passband as possible candidates for a HOM BPM system as this region contains trapped modes that are localised within the cavity. However these initial eigenmode calculations also highlighted the problem that since the majority of the HOMs are above their cut-off frequencies they will propagate throughout the entire module. As a result of the multi-cavity modes there are many more resonances than those predicted by

the single uncoupled cavity calculations; while there are matches with the predicted resonances many of the resonances are shifted away from their uncoupled idealised values. Hence it proved necessary to simulate ACC39 in its entirety.

To facilitate this we utilised the parallel electromagnetic suite of ACE3P, in which we used the eigenmode solver OMEGA3P to calculate the resonances of ACC39 in its entirety up to 10 GHz. Both the 5th dipole and the 1st beampipe passbands were confirmed as being localised within ACC39 and hence possible candidates for a HOM BPM system. These calculations demonstrated the problematic nature of the multi-cavity modes in ACC39.

ACC39 was also simulated in its entirety using the driven modal S3P solver of ACE3P. The simulations from GSM and S3P were shown to be comparable. However we note that in order for GSM to be accurate at least one propagating mode must be present and below the beampipe cutoff of ~4.39 GHz GSM requires a large number of evanescent modes to be included in the calculation to be accurate. Additionally, the CSC scheme was used to determine the S-parameters of the full cavity string. The comparison between measured and simulated data shows a remarkable agreement. The deviations are attributed to not considered effects in the simulation, for example reflections from the input couplers, perturbations of the cavities from their design shape.

The simulations demonstrated that the transmission data from each individual cavity was different; due to the modes being strongly coupled to successive cavities. In effect, the impedance loading of a particular cavity varies depending on the location of the cavity. This will of course make experimental determination of a particular eigenmode a non-trivial process. This is further complicated by the fact that ACC39 is sensitive to fabrication and misalignment errors, particularly the second dipole and the first beampipe band. These misalignment errors shift the idealised multi-cavity resonances. Due to these largely unpredictable frequency shifts in the multi-cavity HOMs in ACC39 it becomes difficult to ascertain the exact nature of any given HOM. Moreover, tests have shown that it is very difficult to locate perturbations in the cavity string based on the transmission factors. Despite this, the 5th dipole band remains a strong candidate for a HOM BPM system within ACC39 due to the localisation of the modes within this band and the diminished sensitivity of this region to fabrication and misalignment errors.

Apart from the described investigations, WP10.5.2 and WP10.5.3 also performed studies of beam excited HOM port signals directly at the FLASH facility. Using an alternative approach in the evaluation electronics delivers promising first results.

ANNEX: GLOSSARY

Acronym	Definition
HOM	Higher Order Modes
GSM	Globalised Scattering Matrix
CSC	Coupled S-Parameter Calculations
CTC	Coupled Transient Calculations
BPM	Beam Position Monitor
FEL	Free Electron Laser
BBU	Beam Blow Up
FEM	Finite Element Method
ALPS	Algorithms and Libraries for Physics Simulations
HFSS	High Frequency Structure Simulator
ACE3P	Advanced Computational Electromagnetics 3P
RMS	Root Mean Square
MWS	Microwave Studio
SVD	Singular Value Decomposition
RSA	Real-time Spectrum Analyzer

http://cern.ch/EuCARD/about/glossary/